Spring 1971

Spectroscopic Measurement of the Electron Temperature in the Tenuous Argon Ion Laser Plasma

Dane Danijel Bicanic
Old Dominion University

SPECTROSCOPIC MEASUREMENT OF THE ELECTRON TEMPERATURE IN THE TENUOUS ARGON ION LASER PLASMA

A THESIS

SUBMITTED TO

THE FACULTY OF THE DEPARTMENT OF PHYSICS

OLD DOMINION UNIVERSITY

In partial fulfillment

of the requirements for the degree of

MASTER OF SCIENCE

BY

DANE DANIJEL BIĆANIĆ

Norfolk, Virginia

January 1971

APPROVAL SHEET

This thesis is submitted in partial fulfillment of the requirements for the degree of Master of Science

Author
Dane Bicanic

Dean, School of Science
Melvin A. Pittman

Chairman, Graduate Council

Supervisory Committee

Chairman Jacob Becher

Wynford Harries

George S. Ofelt

ACKNOWLEDGEMENTS

With great plesure I acknowledge the help and encouragement of Dr. Jacob Becher, my thesis advisor, and Dr. George S. Ofelt and Dr. Wynford L. Harries, members of the thesis committee. Special thanks to Dr. Gary E. Copeland for his time, effort, helpful criticism and dedication in this project. I have enjoyed the fullest co-operation of the engineering students Andrew J. Csomay, John M. Franke, Herbert B. Murrell, Paul L. Goodman, and my physics colleagues Thomas Woodard and Charles A. DeJoseph. I also wish to thank to Nancy and John R. Hall, Jr. for their kind assistance in checking the English grammar and language. My sincere thanks to the Old Dominion University Physics Department for giving me the opportunity to study in this country, and to the Modern Optics and Spectroscopy Laboratory for financial assistance during the course of the study.

Finally, I wish to express the most appreciation to my wife, Vesna, for her faith and support, and to both our families who made this possible.

To my wife, my parents, and the
memory of the late Rudolf Bićanić.

TABLE OF CONTENTS

TABLE OF CONTENTS (Continued)

LIST OF TABLES

LIST OF FIGURES

LIST OF FIGURES(Continued)

LIST OF FIGURES (Continued)

A B S T R A C T

The validity of the line intensity ratio technique for measuring the electron temperature was examined for an argon plasma with a "population inversion" i.e., the number of ions with electrons in the upper 4p levels was greater than in the lower 4s levels. The line intensities from these levels, the argon ion lasing transitions, were measured in a pulsed tenuous plasma at 110μ Hg produced by discharging a capacitor through a tube 2m long and 7mm inside diameter. The electron impact cross sections for simultaneous excitation and ionization as measured by Latimer and St. John were used and averaged over the velocity distribution of electrons, assumed Maxwellian. The electron temperatures obtained, ranged from 1.0 - 1.7 eV depending on which lines were observed. A theory of the positive column, where wall effects are not considered gives values about twice as high as an upper bound.

CHAPTER I

INTRODUCTION

A number of methods exist to determine the electron temperature, which is a measure of the mean kinetic energy of the electron in the plasma(eg. Langmuir probes, electrical resistivity, pressure balance and numerous spectroscopic techniques). The mean kinetic energy E of an electron is related to the electron temperature T_e, as[27]

$$E = \frac{1}{2} m\overline{v^2} = \frac{3}{2} kT_e \quad . \qquad (1\text{-}1)$$

In equation (1-1) $\overline{v^2}$ is the mean square velocity of the Maxwellian electron velocity distribution function; m is the electron mass; and k is the Boltzmann constant.

The aim of this dissertation is to determine the electron temperature in a tenuous argon ion laser plasma by means of the spectroscopic line intensity ratio method. No data on argon ion laser plasmas obtained by this method are yet available. The line intensity technique was originally suggested by Cunningham, who noted that when the electron impact cross section curves for some transitions differ greatly in shape, they may be used to determine the electron temperature by observing the ratio of their line

intensities[7] . Cunningham used Lees' cross sections for 4713 Å (2^3P-4^3S) and 4921 Å (2^1P-4^1D) neutral helium transitions to obtain the intensity ratio as a function of the temperature(Figure 1a), and confirmed the results for the electron temperature obtained by other diagnostic techniques.[25,19] Two basic assumptions were made by Cunningham: first, the electron velocity distribution is Maxwellian; and second, the observed line intensities are proportional to the excitation rate at which the upper levels are populated by the electron collisions with the ground state neutral helium atoms. The later assumption means that the rate of direct excitation exceeds the cascading rates.

In 1964, Sovie successfully applied Cunningham's method to the tenuous helium plasma[23] . His results, shown in Figure 1b, were in the fair agreement with the data obtained by the conventional probe method.

At the present time, the single step excitation and ionization of the neutral argon atoms by the electron impact is thought to be the dominant process in the pulse argon ion laser. Although, the line intensity ratio method does not apply to the case of the stimulated emission(lasing action), the electron temperature of the laser plasma continues to be deduced by suitably blocking the mirrors of the laser cavity in such a way that the laser plasma is produced in the non-lasing mode.

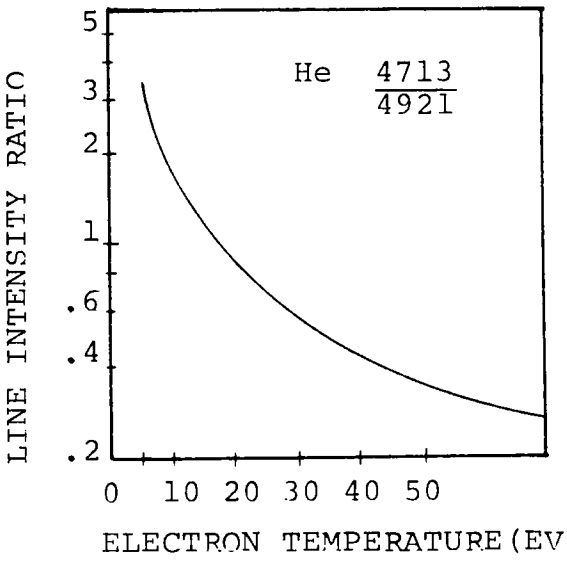

Figure 1a.

Line intensity ratio for helium lines, as calculated by Cunningham.

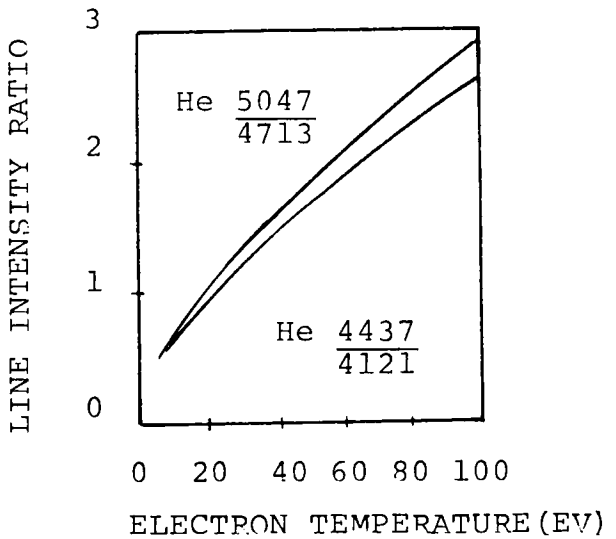

Figure 1b.

Line intensity ratio as a function of electron temperature in the tenuous helium plasma (after Sovie).

We expect that the electron temperature obtained by the line intensity ratio technique will help in understanding the excitation processes and mechanisms present in the argon ion laser plasma. The comparison of the data attained and the results of other diagnostic methods should confirm the feasibility of the line intensity ratio technique in determining the electron temperature in the tenuous plasma in the non-lasing mode.

CHAPTER II

THE SPECTROSCOPIC LINE INTENSITY RATIO TECHNIQUE

1. The derivation of the fundamental line intensity ratio equation

Some of the light emitted from the plasma is composed of spectral lines, resulting from the transitions between the bound energy levels in the atom. The intensity of the light emitted by the non-lasing plasma is proportional to the population density N_j (i.e. the number of atoms per unit volume) of the excited or ionized level j. In general, N_j can be found from the equation

$$\frac{dN_j}{dt} = Z(t) + Z'(t) \quad , \qquad (2\text{-}1)$$

where Z(t) and Z'(t) are the rates of the population and the depopulation of level j, respectively. We use the positive sign in the equation (2-1) to add an implicit negative quantity Z'(t) to Z(t). The main populating processes of the atomic levels in plasma are: collisions of the first and second kind, absorption, recombination, and cascade transitions from higher energy levels. Some of the dominant depopulating processes are spontaneous emission, electron-atom and electron-ion collisions and quenching

atom-wall type collision. Assuming the steady state of the plasma, equation (2-1) is

$$\frac{dN_j}{dt} = 0 \quad , \tag{2-2}$$

or

$$Z(t) + Z'(t) = 0 \quad . \tag{2-3}$$

If the number of the processes contributing to the population increase of the atomic level j is denoted by ΔN_{ij}, and the number of depopulating processes of the same level by $\Delta N'_{jk}$, one infers

$$\Sigma\Delta N_{ij} + \Sigma\Delta N'_{jk} = 0 \quad . \tag{2-4}$$

In equation (2-4) the summation goes over the levels i and k involved in the populating and depopulating processes of level j. In addition, the total number of plasma constituent particles must be conserved, and consequently

$$\Sigma N_j + \Sigma N_i^+ + N_o = N \quad , \tag{2-5}$$

where N_j, N_i^+, and N_o are the population densities of the excited atoms, ions and neutral atoms respectively. The systems of equations (2-4) and (2-5) cannot be solved completely, as there is generally an infinite number of excited states of the atom. Each of the different processes ΔN_{ij} and $\Delta N'_{jk}$ considered in equation (2-4) depends on the effective optical cross section, the electron density, the

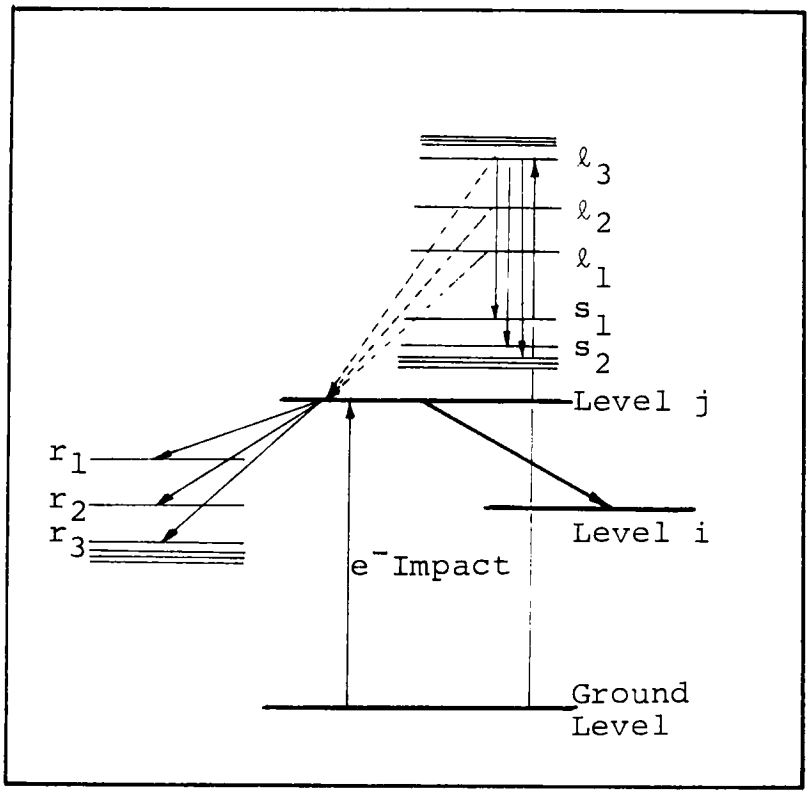

Figure 2.

The general energy level diagram.

velocity distribution of electrons, Einstein's transition probability coefficients, and the population densities of the neutral and excited atoms and the ions.

Assuming that the direct excitation and the cascading transitions are the two dominant populating processes, and spontaneous radiative transition is the sole depopulating mechanism of the level j, the number of unknowns in equations (2-4) and (2-5) is greatly reduced. We can therefore determine the population density N_j in the steady state plasma

At this point, a low pressure chamber containing N_o neutral gas atoms per unit volume is considered. If a beam of determined velocity v is injected into a collision chamber, the production rate for the level j(i.e. the number of direct o-j excitations per unit volume and unit time leading to the population of level j) is defined as

$$N_j = N_o \, Q_{oj}(v) \, n_e(v) \quad . \qquad (2\text{-}6)$$

In equation (2-6) N_o, is the population density of the neutral gas atoms in the ground state, $Q_{oj}(v)$ is the level excitation cross section for the excitation from the ground state of the neutral atom to the excited level j, and $n_e(v)$ is the flux density of the electrons(i.e. number of electrons in the beam passing through unit area per unit time). Including the cascading processes from all upper levels ℓ to level j and the radiative spontaneous transitions from level j to lower levels r(Figure 2) with the direct

excitation process, one deduces for $\dot{N}_j$ [9]

$$\dot{N}_j = N_o\, Q_{oj}(v)\, n_e(v) + \sum_{\ell=j+1}^{\infty} N_\ell A_{\ell j} - N_j \sum_{r=0}^{j-1} A_{jr}. \quad (2\text{-}7)$$

A_{jr} and $A_{\ell j}$ are Einstein's transition probability coefficients for transitions between j-r and ℓ-j levels. The first two terms on the right hand side of the equation(2-7) represent the net population gain, and the third negative term accounts for the total population loss due to the spontaneous transitions from level j. In the case of the steady state, the net gain equals the net loss of population, and the population density N_j can be found from equation (2-7), as

$$N_j = \frac{N_o\, Q_{oj}(v)\, n_e(v) + \sum_{\ell=j+1}^{\infty} N_\ell\, A_{\ell j}}{\sum_{r=0}^{j-1} A_{jr}} . \quad (2\text{-}8)$$

Another atomic level i lying below level j is now considered. The transition is assumed to take place from the j-th to the i-th level emitting the photon of the frequency ν_{ji}. When the stimulated radiative transitions are neglected, the energy W_{ji} radiated at the frequency ν_{ji} per unit time and unit volume is given by

$$W_{ji} = N_j\, A_{ji}\, h\nu_{ji} \quad , \quad (2\text{-}9)$$

where h is the Planck constant.

Substituting the expression for N_j from equation(2-8) into the equation(2-9), the radiated energy W_{ji} is obtained as

$$W_{ji} = \frac{N_o\, Q_{oj}(v)\, n_e(v)\, A_{ji}\, h\nu_{ji}}{\sum_{r=0}^{j-1} A_{jr}} + \frac{\sum_{\ell=j+1}^{\infty} N_\ell\, A_{\ell j}\, A_{ji}\, h\nu_{ji}}{\sum_{r=0}^{j-1} A_{jr}} , \quad (2\text{-}10)$$

which can also be written as

$$W_{ji} = \frac{N_o\, n_e(v)\, A_{ji}}{\sum_{r=0}^{j-1} A_{jr}} \left\{ Q_{oj}(v) + \frac{\sum_{\ell=j+1}^{\infty} N_\ell\, A_{\ell j}}{N_o\, n_e(v)} \right\} h\nu_{ji} . \quad (2\text{-}11)$$

Assuming that the direct excitation process is the dominant populating mechanism, one expresses the population density N_ℓ of any excited level ℓ in the same manner as in deriving the equation(2-8). We assume here that the spontaneous transitions from level ℓ account for the population loss of N_ℓ, and the cascading processes from the upper levels to level ℓ are small, and therefore can be neglected. The cascading processes to level ℓ represent only the second order contribution in the population density of the level j. Thus, the rate of the population density $\dot{N}_\ell$ in the steady state is obtained by

$$\dot{N}_\ell = N_o\, Q_{o\ell}(v)\; n_e(v) - N_\ell \sum_{s=0}^{\ell-1} A_{\ell s} = 0 \ , \qquad (2\text{-}12a)$$

or

$$N_\ell = \frac{N_o\, Q_{o\ell}(v)\; n_e(v)}{\sum_{s=0}^{\ell-1} A_{\ell s}} = c_\ell\, N_o\, n_e(v) \ , \qquad (2\text{-}12b)$$

where

$$c_\ell = \frac{Q_o\ (v)}{\sum_{s=0}^{\ell-1} A_{\ell s}} \ , \qquad (2\text{-}12c)$$

and is a constant. Using the equation(2-12c), the second term in the brackets of the equation(2-11) can be written as

$$\frac{\sum_{\ell=j+1}^{\infty} N_\ell\, A_{\ell j}}{N_o\, n_e(v)} = \frac{c_\ell\, N_o\, n_e(v)\, A_{\ell j}}{N_o\, n_e(v)} \ , \qquad (2\text{-}13)$$

and the equation(2-11) is taking the form

$$W_{ji} = \frac{N_o\, n_e(v)\, A_{ji}}{\sum_{r=0}^{j-1} A_{jr}} \left\{ Q_{oj}(v) + \sum_{\ell=j+1}^{\infty} c_e\, A_{\ell j} \right\} h\nu_{ji} . \qquad (2\text{-}14)$$

The sum of the two terms appearing in the brackets of the equation(2-14) is defined as the apparent cross section $Q'_j(v)$ of level j, or

$$Q'_j(v) = Q_{oj}(v) + \sum_{\ell=j+1}^{\infty} c_\ell A_{\ell j} \quad . \tag{2-15}$$

Using the relation(2-15) in the equation for the radiated energy W_{ji}(2-14), one obtains

$$W_{ji} = \frac{N_o n_e(v) A_{ji} Q'_j(v)}{\sum_{r=0}^{j-1} A_{jr}} h\nu_{ji} \quad . \tag{2-16}$$

Introducing the branching ratio B_{ji}, defined as

$$B_{ji} = \frac{A_{ji}}{\sum_{r=0}^{j-1} A_{jr}} \quad , \tag{2-17}$$

one can rewrite equation(2-16) as

$$W_{ji} = N_o n_e(v) B_{ji} Q'_j(v) h\nu_{ji} \quad . \tag{2-18}$$

The product of the branching ratio B_{ji} and apparent cross section $Q'_j(v)$ is termed as the effective optical cross section $Q_{ji}(v)$ for the j-i transition

$$Q_{ji}(v) = B_{ji} Q'_{ji}(v) \quad . \tag{2-19}$$

The electron flux density $n_e(v)$ can now be expressed in terms of the electron density N_e and the velocity of the electron v

$$n_e(v) = N_e v \ . \qquad (2\text{-}20)$$

Using the relations (2-19) and (2-20) in the equation (2-18), one obtains

$$W_{ji} = N_o \, N_e \, Q_{ji}(v) \, v \, h\nu_{ji} \ . \qquad (2\text{-}21)$$

The intensity I_{ji} of the j-i transition is found by dividing the radiated energy W_{ji} by $h\nu_{ji}$, namely

$$I_{ji} = \frac{W_{ji}}{h\nu_{ji}} = N_o \, N_e \, Q_{ji}(v) \, v \ , \qquad (2\text{-}22)$$

and it has the dimension of the inverse volume per unit time.

2. The concept of the folded cross section

The equation(2-22) was derived in the assumption that the monoenergetic beam of the electrons is injected into the low pressure gas in the collision chamber. However, one often deals with the distribution of the electron velocities, and the equation(2-22) becomes

$$I_{ji} = N_o \, N_e \, \langle Q_{ji}(v) \, v \rangle \ , \qquad (2\text{-}23)$$

where the angle brackets indicate that the effective optical cross section $Q_{ji}(v)$ for j-i transition is averaged over the velocity distribution function.[23] This procedure is sometimes refered to as the folding of the cross section, or explicitly (if $\int_0^\infty f(v)dv$ is normalized to one)[22,9]

$$< Q_{ji}(v)\ v > = \int_{v_j}^{\infty} Q_{ji}(v)\ f(v)\ v\ dv\ . \qquad (2\text{-}24)$$

In the equation (2-24), f(v) is the velocity distribution function of the electrons and v is the electron velocity. The velocity v_j appearing as the lower limit of the integration corresponds to the j-th excitation treshold energy value. The integral in the equation (2-24) involves three different functions of the electron velocity. The Maxwelliar distribution function f(v) and the electron velocity v originate at zero value for the electron velocity, whereas the excitation cross section onset v_j is at some greater velocity. The relation (2-24) has a vanishining value for any velocity v ranging from zero to v_j. The electron temperature corresponding to the Maxwellian distribution determines the number of the electrons in the distribution tail with sufficient energy to perform a direct excitation and ionization. The percentage of the total number of electrons whose speeds exceed the treshold velocity v_j is given by[20]

$$\frac{N_{x\to\infty}}{N} \cdot 100 = [1-\mathrm{erf}(x) + \frac{2}{\sqrt{\pi}} \exp(-x^2)\cdot x]\cdot 100. \quad (2\text{-}25)$$

In equation(2-25)

$$x = \frac{v_j}{v_m} \quad , \quad (2\text{-}26)$$

where v_m is the most probable velocity[22]

$$v_m = \left(\frac{2kT}{m}\right)^{1/2}. \quad (2\text{-}27)$$

The most probable velocity v_m is related to the mean velocity $\bar{v}$

$$v_m : \bar{v} = 1 : 1.128 \ . \quad (2\text{-}28)$$

3. The line intensity ratio method as a technique for determination of the electron temperature

In the first part of this chapter, the equation for the calculation of the line intensity (2-23) was derived. We consider now the two transitions j—i and k—ℓ. Using the equation(2-23), one can write

$$I_{ji} = N_o N_e < Q_{ji}(v)\ v > \ , \quad (2\text{-}29)$$

and

$$I_{k\ell} = N_o N_e < Q_{k\ell}(v)\ v > \qquad (2\text{-}30)$$

for the line intensities of these transitions.

Taking the ratio R of the two intensities, one has:

$$R = \frac{I_{ji}}{I_{k\ell}} = <Q_{ji}(v)\ v> / < Q_{k\ell}(v)\ v >, \qquad (2\text{-}31)$$

or in other words, the ratio of the line intensities R of the two transitions is equal to the ratio of the folded cross sections for the same transitions. As the folded cross section involves the electron velocity distribution function, which defines the temperature, it follows that the ratio R is also a function of the electron temperature T_e. Therefore, if the effective optical cross section for a certain transition is known, one is able to obtain the folded cross section (equation 2-24) for any desired temperature of the electron velocity distribution function and to plot it as a function of the electron temperature. The folding procedure is done for several transitions in such a way that a number of curves representing the line intensity dependence on the electron temperature is obtained. Any of the two transitions making the ratio R must be either neutral or ionic, such that the electron density and the

neutral gas density do not appear in equation(2-31), and consequently R is only dependent on the electron temperature T_e. The curves showing the functional dependence of the line intensity ratio R on the electron temperature T_e can simply be found by dividing any two of the $I=f(T_e)$ curves available.(I refers to the intensity of an arbitrary transition)

One can also spectroscopically measure the line intensities of the same transitions for which the folded cross sections are known. The experimentally determined intensities I_{ji} and $I_{k\ell}$ can be used to calculate the ratio

$$R' = \frac{I_{ji}}{I_{k\ell}} .$$

The electron temperature is than found by reading the value of T_e, which is corresponding to the experimentally determined ratio R' from the previously obtained curves $R = f(T_e)$.

CHAPTER III

ARGON ION LASER

As mentioned in the introduction, the purpose of this study is to determine the electron temperature in the tenuous argon ion laser plasma. The argon ion laser is basically a three level system consisting of an upper and lower laser level, and a third level serving as a reservoir. The third level is either an excited neutral level or an ion ground state. In some cases, depending on the type of the excitation mechanism, the neutral metastable state, as well as the ionic metastable state can be used as a third laser level.[2]

In this work we have restricted ourselves to a single step excitation and ionization, and used Latimer's and St. John's cross sections to determine the electron temperature. However, we shall first consider the various suggested excitation mechanisms leading to the population inversion in the 4p, 4s levels of the argon ion laser. Each of these suggested mechanisms are characterized by the appropriate cross sections.

The determination of the electron temperature by the line intensity ratio technique is based on the knowledge of

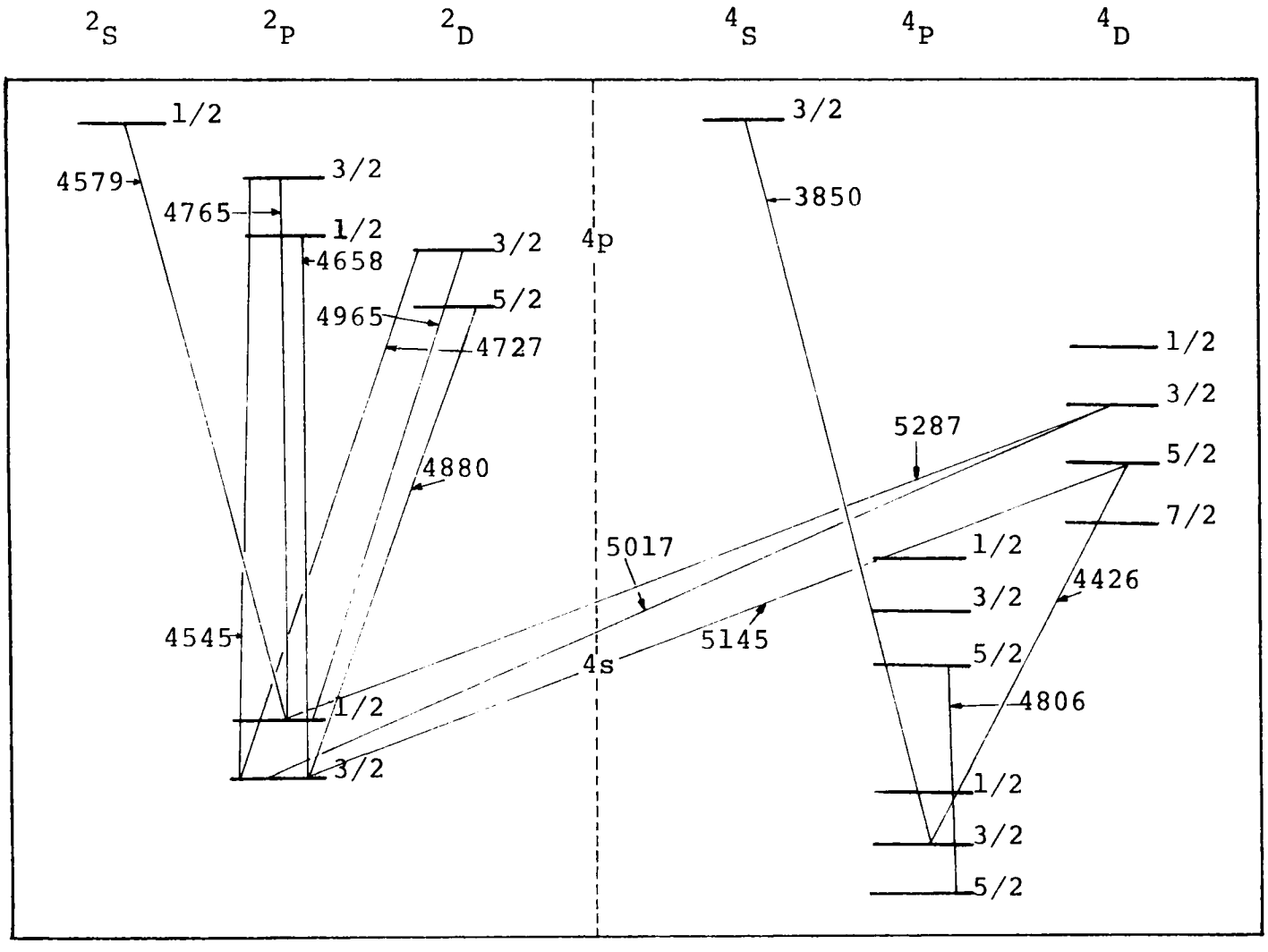

Figure 3.

Important 4p and 4s energy levels and transitions in argon ion laser

the cross sections. Therefore, the electron temperature is strongly dependent on the type of the mechanism by which the population inversion is achieved in 4p, 4s levels of the argon ion laser; 4p-4s transitions are shown in Figure 3.

1. Upper laser level excitation mechanisms

Step excitation

Labuda, Gordon and Miller have proposed a double step excitation as a mechanism for the population of the upper laser levels in the argon ions[16]. During the first stage of the double excitation process, the ground argon ions are created by collisions of electrons with ground state neutral argon atoms. Schematically, this process is shown in Figure 4a. The population density of the upper laser levels is proportional to the square of the electron density in a double excitation process. Consequently, the population density of the upper laser levels is proportional to the square of the current.

Single step excitation

Bennett suggested, and Koozekanani theoretically investigated a direct, one step excitation and ionization from the neutral ground state of the argon, to the upper laser states, as the dominant process for the population

of the upper laser states[4,14]. This process is thought to take place in pulsed lasers, where large values of the ratio of the electric field strength E to the pressure p are required to give electrons sufficient energy to ionize the argon atoms. The population density of the upper level is expected to be directly proportional to the electron density and current. Bennett's excitation scheme is illustrated in Figure 4b.

Excitation from the ion metastable state

As suggested by Labuda et al., this mechanism assumes that the population of the upper laser states is achieved by the excitation of the metastable ions[17]. The first excited state of the metastable ion is populated in two different ways: a) the double step process consisting of the excitation from the neutral ground state to the ion ground state, followed by the excitation to the first metastable ion state(Figure 4c), b) spontaneous radiation from the higher energy levels, previously excited by means of the double step process(Figure 4d). In both of these, the population density of the metastable ion level is expected to be proportional to the electron density squared.

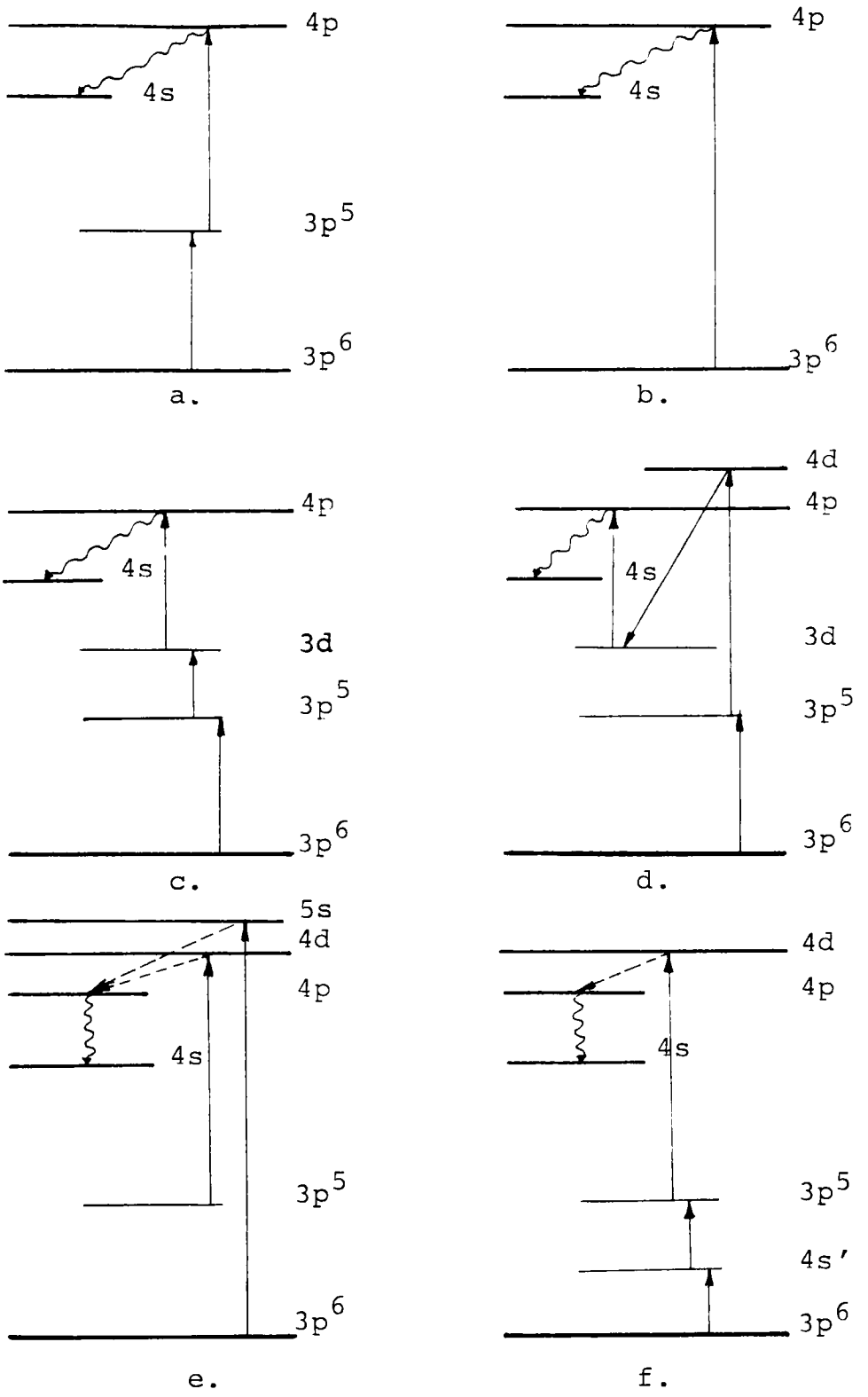

Figure 4.

Different excitation mechanisms in argon ion laser.

Cascading from 4d, 5s levels to the upper laser states

Rudko and Tang attributed the population of the 4p laser levels to the strong spontaneous emission from 4d and 5s energy levels(Figure 4e)[21]. These levels from which spontaneous emission takes place are assumed to be populated by a double step excitation process, and therefore their population is proportional to the electron density squared.

Excitation from the neutral metastable state

The excitation from the metastable neutral state(Figure 4f), rather than from the ion metastable level(Labuda, Figure 4c), was suggested by Koozekanani[15]. His theoretical results show that the metastable states $3p^5\ 4s'[1/2]^\circ$ and $3p^5\ 4s[3/2]^\circ$, due to their small ionization treshold energies and large cross sections,would represent favorable levels for the ionization to take place. The first stage of the process originates at the neutral metastable level and terminates at the ground state of the ion. The second stage involves the excitation of the ion ground state to the upper lying states 4d, 5s etc., and the subsequent spontaneous emission from these levels to 4p laser levels.

2. Lower laser level

The rate of depopulation of the lower laser state

has to be greater than the corresponding population rate for the upper laser level, in order to achieve inversion and to maintain the laser action. The transitions $4p\text{-}3p^5$ from the upper laser levels to the ion ground state are optically forbidden. On the other hand, the transition $4s\text{-}3p^5$ is quite favorable, and the depopulation of lower laser levels 4s is achieved by the strong ultraviolet transition. The order of magnitude of the transition probability for the 4p-4s transitions is much smaller than for the $4s\text{-}3p^5$ transitions.[28] Consequently, the lifetimes for 4p states are longer than 4s lifetimes, and the population inversion is attained, provided there are equivalent supply rates for 4s and 4p levels. The depopulating process for 4p levels is shown below:

$$(\text{Ar II})_{4p} \xrightarrow{5000\ \text{Å}} (\text{Ar II})_{4s} \xrightarrow{700\ \text{Å}} (\text{Ar II})_{3p^5}$$

3. Electron excitation cross sections pertinent to the upper argon ion laser states

Several investigators have measured the single step excitation cross sections pertinent to the upper states of the pulsed argon ion laser.[3,5,10,18] We depend on the most

recent effective optical cross section data for eight 4p-4s lasing transitions obtained by Latimer and St. John[18]. These transitions are as follows:

Wavelength (Å)	Transition		Maximum effective optical cross section (10^{-20} cm^2)	Electron energy at the peak (eV)
	upper level	lower level		
3850.58	$4p\,^4S_{3/2}$	$4s\,^4P_{3/2}$	6.8	54.0
4426.01	$4p\,^4D_{5/2}$	$4s\,^4P_{3/2}$	36.0	54.0
4579.35	$4p\,^2S_{1/2}$	$4s\,^2P_{1/2}$	18.0	54.0
4657.89	$4p\,^2P_{1/2}$	$4s\,^2P_{3/2}$	40.0	90.0
4764.86	$4p\,^2P_{3/2}$	$4s\,^2P_{1/2}$	52.0	90.0
4806.02	$4p\,^4P_{5/2}$	$4s\,^4P_{5/2}$	34.0	54.0
4879.86	$4p\,^2D_{5/2}$	$4s\,^2P_{3/2}$	59.0	54.0
4965.07	$4p\,^2D_{3/2}$	$4s\,^2P_{1/2}$	17.0	54.0

It appears that the cross section curves for the eight lasing transitions resemble one of two different functions. The first function exhibits the sharp increase in the cross section values, as the electron energy is increased from the onset value. The peak of the cross section curve is at 54 eV of electron energy; the further increase of the electron energy results in a fast monotonic decrease of the cross

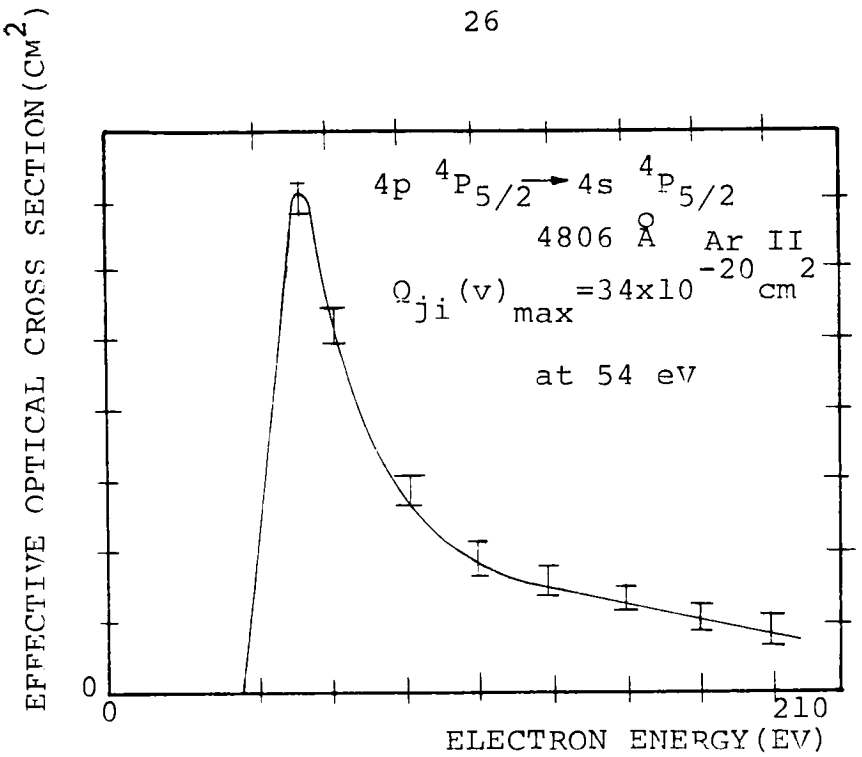

Figure 5.

The"sharp" cross section curve (after Latimer and St. John).

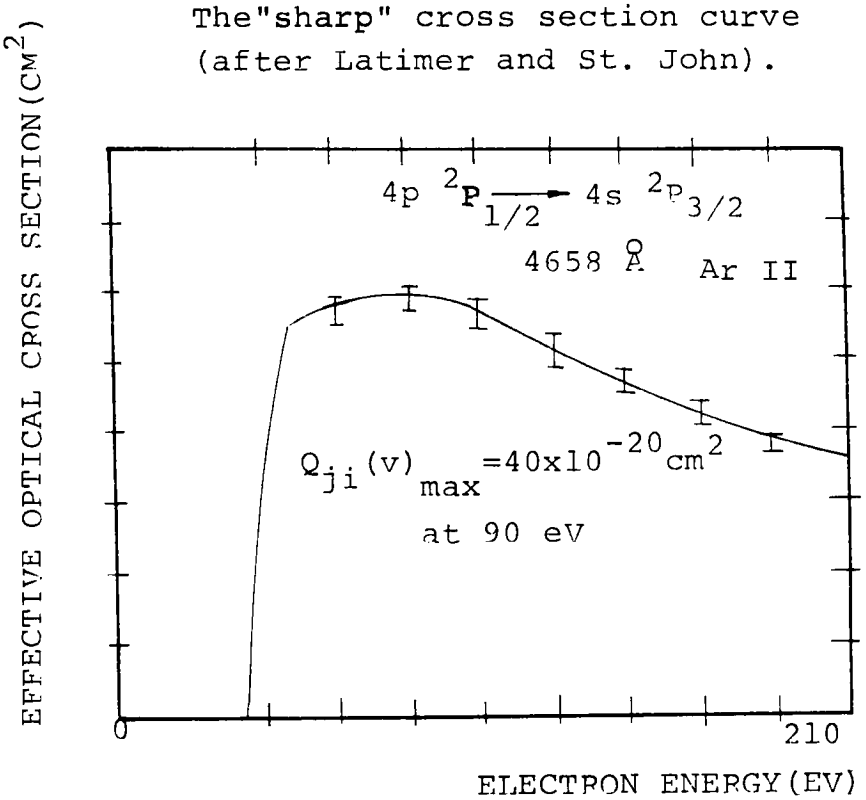

Figure 6.

The"broad maximum"cross section curve (after Latimer and St. John).

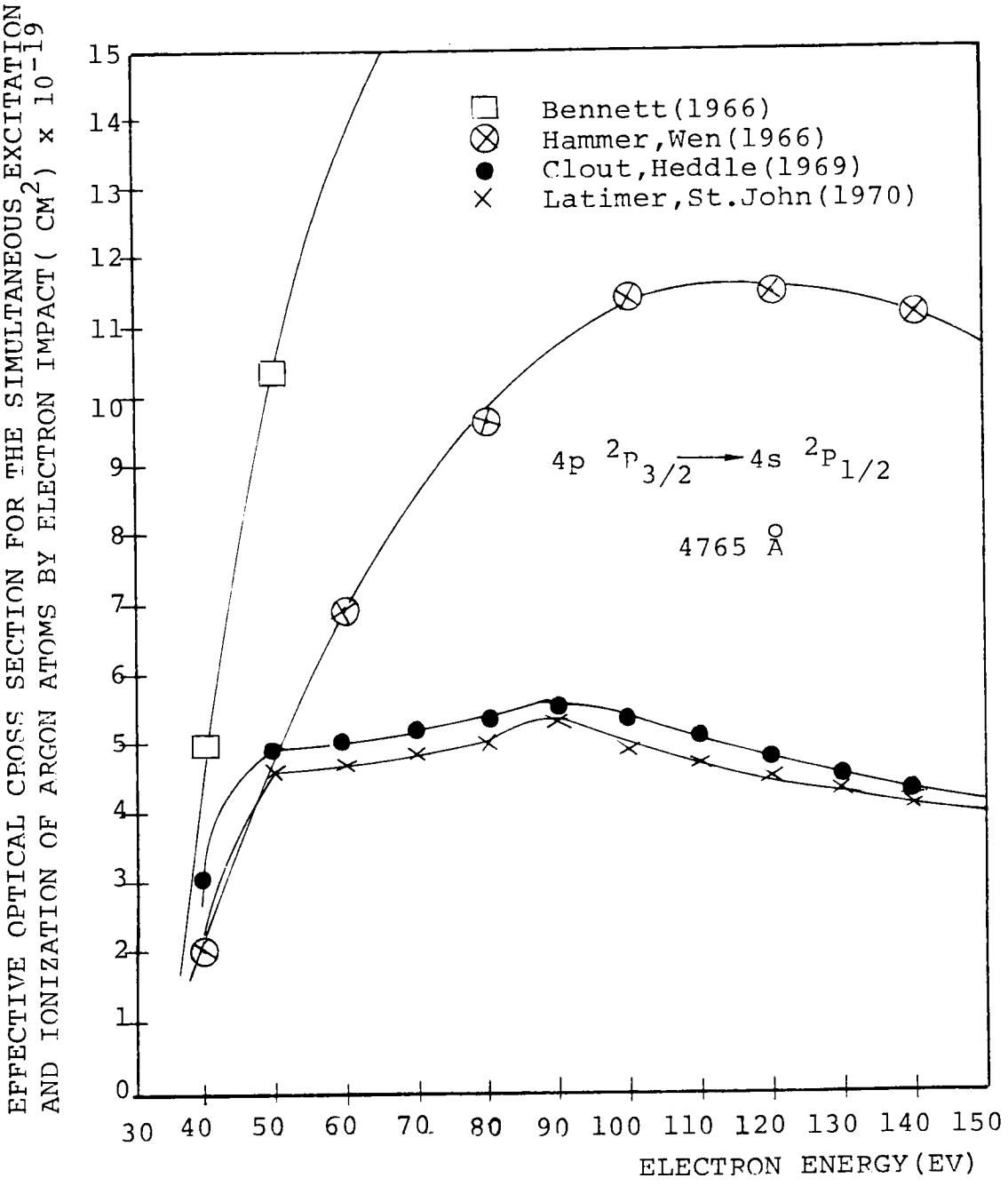

Figure 7.

Measured direct excitation cross sections.

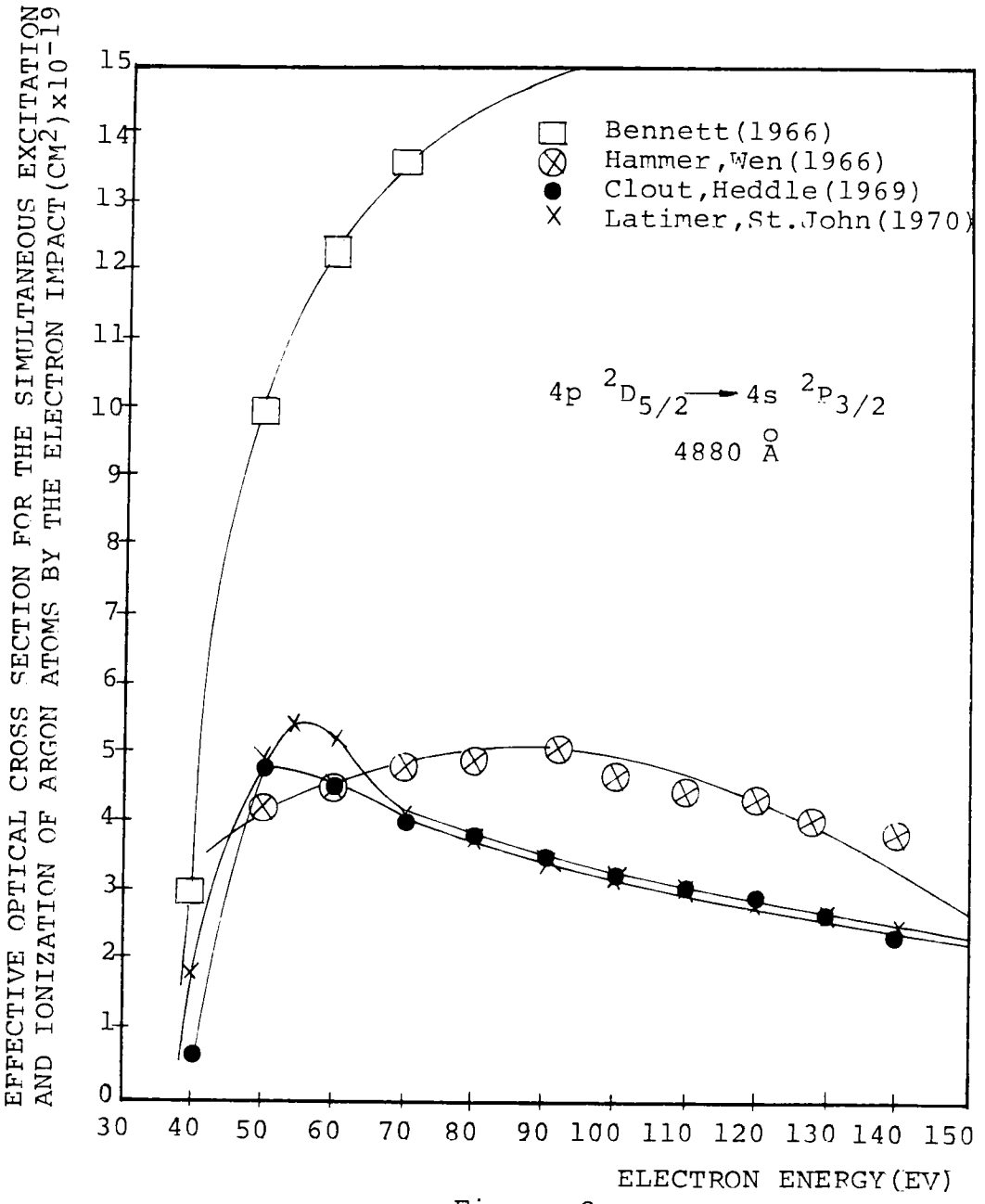

Figure 8.

Measured direct excitation cross sections.

section values(Figure 5). The second function has the broad plateau maximum at 90 eV. Unlike the first function, this one decreases linearly with electron energy beyond the plateau (Figure 6). The cross section data, obtained by Bennett, Clout and Heddle, and Hammer and Wen are compared to Latimer's and St. John's, as represented in Figure 7 and Figure 8. Whereas Latimer's and St. John's data are in very good agreement with Clout's and Heddle's work, large discrepancies are observed regarding other investigators results. The dicrepancies are attributted to relatively high pressure in the collision chamber which may result in a multiple collisional effect and will tend to increase the effective optical cross section [18]. Latimer's and St. John's data have recently been reproduced by another independent group of investigators.[1]

We conclude that the cross sections of Latimer and St. John are probably the most accurate; and we shall average them over the Maxwellian electron velocity distribution to obtain the folded cross sections as a function of the electron temperature. The sole availability of the folded cross sections, as mentioned in chapter II, section 3, does not enable one to determine the electron temperature, because the additional spectroscopic line intensity measurement is also required.

CHAPTER IV

EXPERIMENTAL APPARATUS

In order to obtain the accurate line intensity values (i.e. the photon rate from the excitation region) needed to determine the electron temperature, the experimental detection system has to be calibrated with a known photon rate from a standard lamp.

In this chapter we discuss the calibration procedure and the components of the detection system. The description of the argon ion laser and its constituent parts is given in the last two sections of this chapter.

1. The intensity calibration of the detection system

The intensity calibration procedure of the detection system was used, as described by Jobe.[12] (Figure 9)

We consider now the source of radiation emitting photons of wavelength λ_o into the solid angle Ω_B. The detector system consisting of the quartz lens and the monochromator with the photomultiplier tube will give an output signal I_B in amperes, which is directly proportional to the incident photon rate. The proportionality constant of the detection system is termed

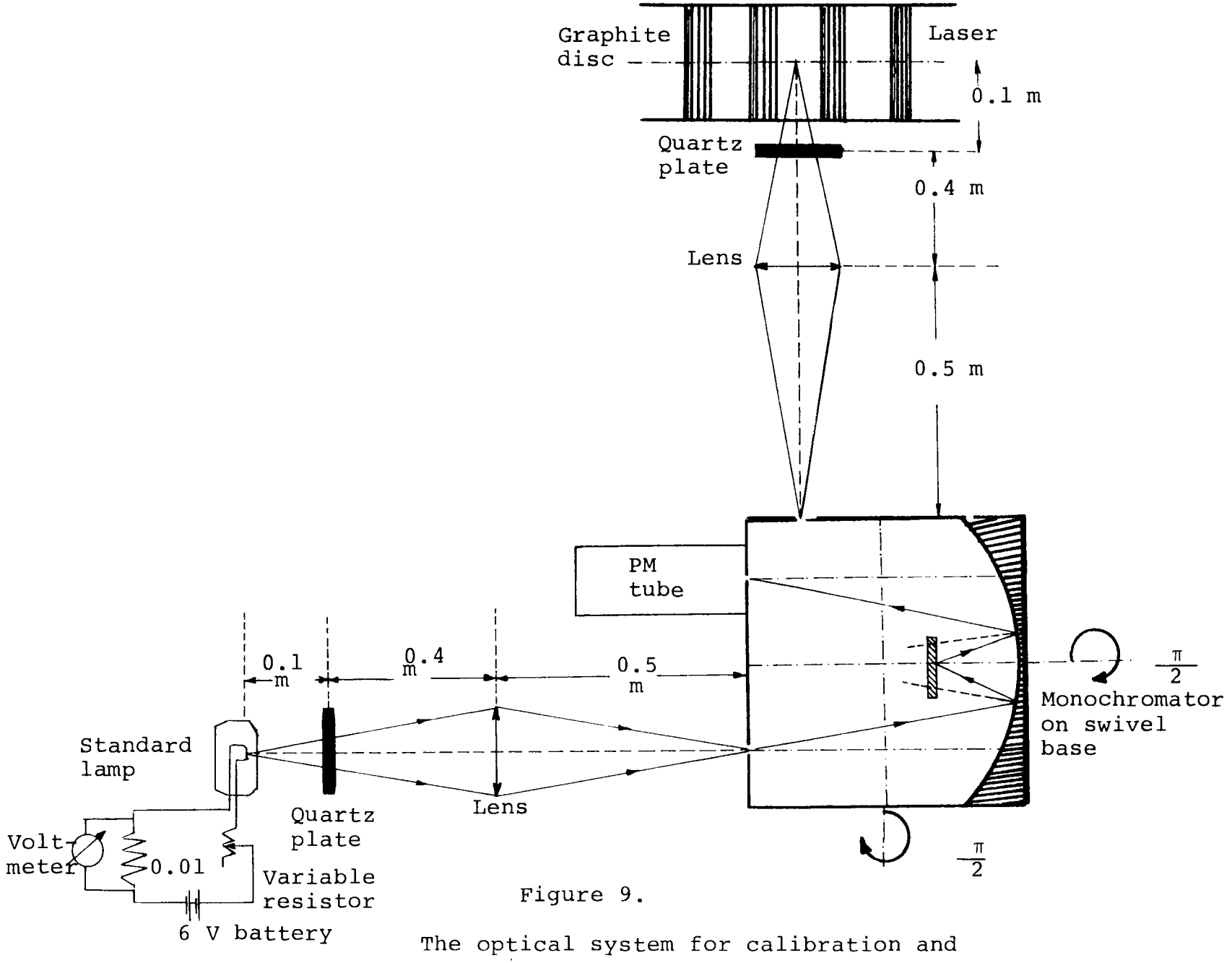

Figure 9.

The optical system for calibration and

Assuming that the photon rate emitted by the tungsten ribbon at the temperature T is a constant over the wavelength interval $2\Delta\lambda$, one can find the amount of radiation transmitted by the triangular bandpass monochromator by using Planck's radiation law and the emissivity values for the tungsten surface. This approximation is good if $\Delta\lambda<100$ Å, $T<3000^{\circ}K$ and $\lambda_o>2200$ Å. The amount of radiation incident on a triangular bandpass of half width $\Delta\lambda$ has to be integrated over the transmission function $T(\lambda)$, defined as

$$T(\lambda) = 1 + \frac{\lambda-\lambda_o}{\Delta\lambda} \quad \text{for } \lambda_o-\Delta\lambda < \lambda<\lambda_o \qquad (4\text{-}4a)$$

and

$$T(\lambda) = 1 - \frac{\lambda-\lambda_o}{\Delta\lambda} \quad \text{for } \lambda_o < \lambda < \lambda_o+\Delta\lambda. \qquad (4\text{-}4b)$$

The spectral radiance from the tungsten ribbon is proportional to the spectral radiance of a black body (the proportionality constant is the emissivity $e(\lambda_o,T)$. Therefore, the expression for $P_{\Delta\lambda}$ can be written as

$$P_{\Delta\lambda} = e(\lambda_o,T) \frac{c}{\lambda_o^4 (e^{c_2/\lambda_o T} - 1)} 2\Delta\lambda , \qquad (4\text{-}5)$$

where c is a velocity of light and c_2 is the second radiation constant.

Jobe has calculated P_{16} for $\Delta\lambda$= 16 Å for 1400-3000°K temperature interval in steps of 200°K [24]. The wavelength λ_o ranges from 2200 Å to 7000 Å, in steps of 20 Å and the emissivity values for tungsten were taken from DeVos [8].

$P_{\Delta\lambda}$ for arbitrary $\Delta\lambda$, in terms of P_{16}, can be expressed as

$$P_{\Delta\lambda} = \frac{P_{16}}{16\ \text{Å}} \Delta\lambda \ . \qquad (4\text{-}5a)$$

The monochromator bandpass of half width $\Delta\lambda$ can be written in terms of the known experimental parameters,

$$\Delta\lambda = \frac{s}{f} \frac{d\lambda}{d\theta} \ , \qquad (4\text{-}6)$$

where f is a focal length of the primary monochromator mirror, s is the entrance and the exit slit width, and θ is the angle between the direction of the exit slit and the normal to the grating. The grating equation for the first order spectrum is

$$d \sin\theta = \lambda \ , \qquad (4\text{-}7)$$

where d is the separation of two grooves. Differentiating expression (4-7), with

$$d = \frac{1}{N_g} \ , \qquad (4\text{-}8)$$

where N_g is a ruling density of the grating, one obtains for equation (4-6)

$$\Delta\lambda = \frac{1}{N_g} \cos\theta \frac{s}{f} \quad . \tag{4-9}$$

Substituting equation (4-9) into equation (4-5a), the following form is obtained

$$P_{\Delta\lambda} = \frac{s}{f\ N_g\ \ 16\ \mathring{A}} \cos\theta\ P_{16} \ . \tag{4-10}$$

Because all of the quantities in the above relation are the constants of the experimental system, it follows that $P_{\Delta\lambda}$ is also a constant for the given $\Delta\lambda$ and the temperature T. Substituting equation (4-10) into equation (4-3) one has

$$I_{ph}(k-j) = \frac{s\ \ P_{16}\ \ 1}{f\ \ 16\ \mathring{A}\ N_g} \cos\theta \frac{\Omega_{SL}}{\Omega_B}\ A_o\ 4\pi\ \frac{I_B}{I_{SL}} \tag{4-11}$$

where $I_{ph}(k-j)$ has the dimension of the reciprocal volume per unit time.

Using identical solid angles for measuring I_B and I_{SL}, and introducing the constant B

$$B = \frac{s}{f\ 16\ \mathring{A}\ N_g} \cos\theta\ A_o\ 4\pi \quad , \tag{4-12}$$

one can write equation (4-11) as

$$I_{ph}(k-j) = B \frac{I_B}{I_{SL}} P_{16} \cdot \qquad (4\text{-}13)$$

Also, substituting relation (4-1) for $I_{ph}(k-j)$ into equation (4-11), one has for the efficiency $\varepsilon(\lambda_o)$

$$\varepsilon(\lambda_o) = \frac{\Omega_{SL} A_o s \cos\theta}{f N_g 16 \mathring{A}} \frac{P_{16}}{I_{SL}} . \qquad (4\text{-}14)$$

With equation (4-12), this reduces to

$$\varepsilon(\lambda_o) = \frac{B}{4\pi} \Omega_{SL} \frac{P_{16}}{I_{SL}} , \qquad (4\text{-}15)$$

or introducing a new constant D,

$$D = B \frac{\Omega_{SL}}{4\pi} , \qquad (4\text{-}15a)$$

one finally has

$$\varepsilon(\lambda_o) = D \frac{P_{16}}{I_{SL}} . \qquad (4\text{-}16)$$

As P_{16} and I_{SL} both depend on the wavelength and the temperature, one obtains the efficiency $\varepsilon(\lambda_o)$, as a function of wavelength for different temperatures T. The efficiency of the detection system should not depend on temperature.

Once the efficiency was found as a function of the wavelength(using equation 4-16), and was shown to be independent of the temperature(the procedure described in Chapter V), the absolute line intensity can be calculated from the measured relative line intensity. The multiplicative constant D appearing in the equation (4-16) is not of interest, because in the line intensity ratio technique we consider only the ratios of spectral lines, and not the individual absolute intensities.

2. Photomultiplier and monochromator

The experimental set up(Figure 9) consisted of a detector photomultiplier tube 9558QB, manufactured by EMI, with an S-20 spectral response. A special photomultiplier base with equal resistors, and therefore an equal potential drop across all the dynodes, was designed and used. The last few stages of the base had capacitors included in addition, such that the frequency response was enhanced. The photomultiplier was powered by a Fluke d.c. power supply at 1310 Volts, which was well stabilized, and was never turned off during the course of the experiment. The monochromator used was a 1/2 m Jarrell-Ash, Fastie-Ebert mount with curved slits to enhance the separation of spectral lines. It was mounted on a swivel base, such that one could alternatively observe the light from the laser or the standard lamp(Figure 9).

3. Standard lamp

The standard lamp, manufactured by General Electric, was a 30 A/ 6 V/ T24 ribbon filament lamp[13]. The filament was mounted 1 meter from the entrance slit of the monochromator. The image optics for observing the standard lamp and a laser were identical. To compensate for the laser light loss due to the absorption by the quartz plate on its path, an identical quartz plate was inserted in front of the standard lamp(Figure 9). The standard lamp requires approximately 6 V and 15-40 A for its proper operation, which was supplied by a large 148 Amperhour, 6 V battery and a variable resistor. The current through the lamp was monitored by measuring the voltage drop across a precision 0.01Ω resistor with a digital voltmeter, noting that all time variations in current were kept down to less than 0.01 A. The experimental technique was essentially the following: the standard lamp was turned on, stabilized and adjusted in temperature by using a vanishing filament optical pyrometer. Once the desired temperature stability is achieved, the monochromator was set to the wavelength 5000 Å. The recorder was adjusted for maximum deflection at this wavelength, and the d.c. output from the photomultiplie

tube was measured. Then, the wavelength of the monochromator was changed to 3500 Å and the dark current was measured. The spectral intensity was detected in 3500-5500 Å range by the monochromator system and measured as a function of wavelength(all argon ion laser transitions are also in this wavelength interval).

4. Laser

The laser cavity, an almost confocal resonator, was a meter and a half long and it varied from run to run. The bore diameter of the laser tube was kept at 7mm. The laser was equipped, as most ion lasers, with quartz Brewster windows. In order to obtain a high degree of ionization for the transitions between ionic states, high current was required. This was done by discharging the capacitors through a series of graphite discs, with the holes in the discs, such that the current was constrained to flow through a series of coaxial identical holes. Graphite was chosen for its high thermal conductivity, low sputtering rate and high melting point. The power supply for the argon ion laser was capable of 11 A d.c. at 3000 V. The excitation block scheme for the laser is given in Figure 10. The pulser was principally a periodically excited auto coil which produced a preionization of the plasma just previous to the main application of the power supply.

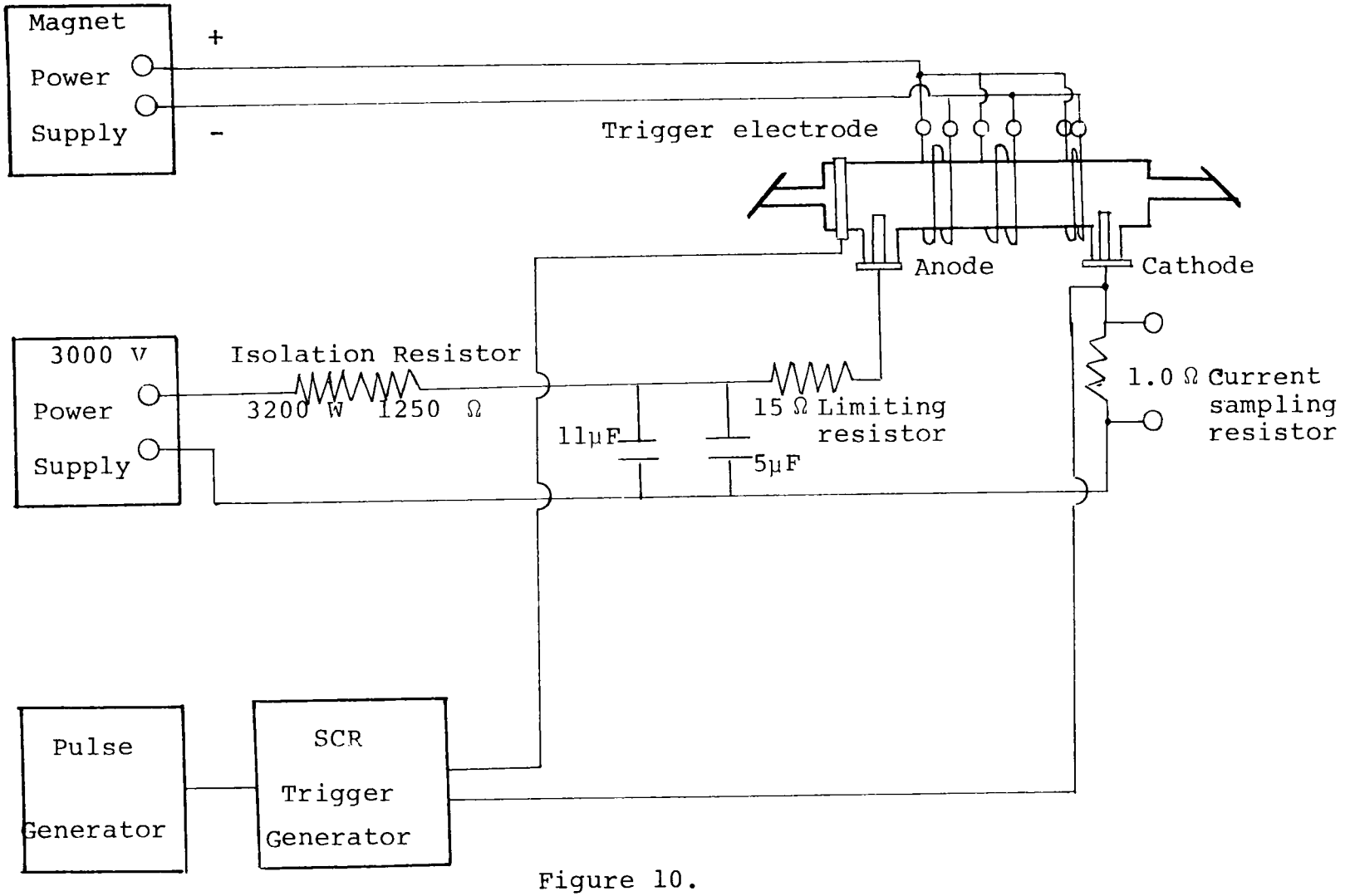

Figure 10.

The excitation block scheme for the argon ion laser.

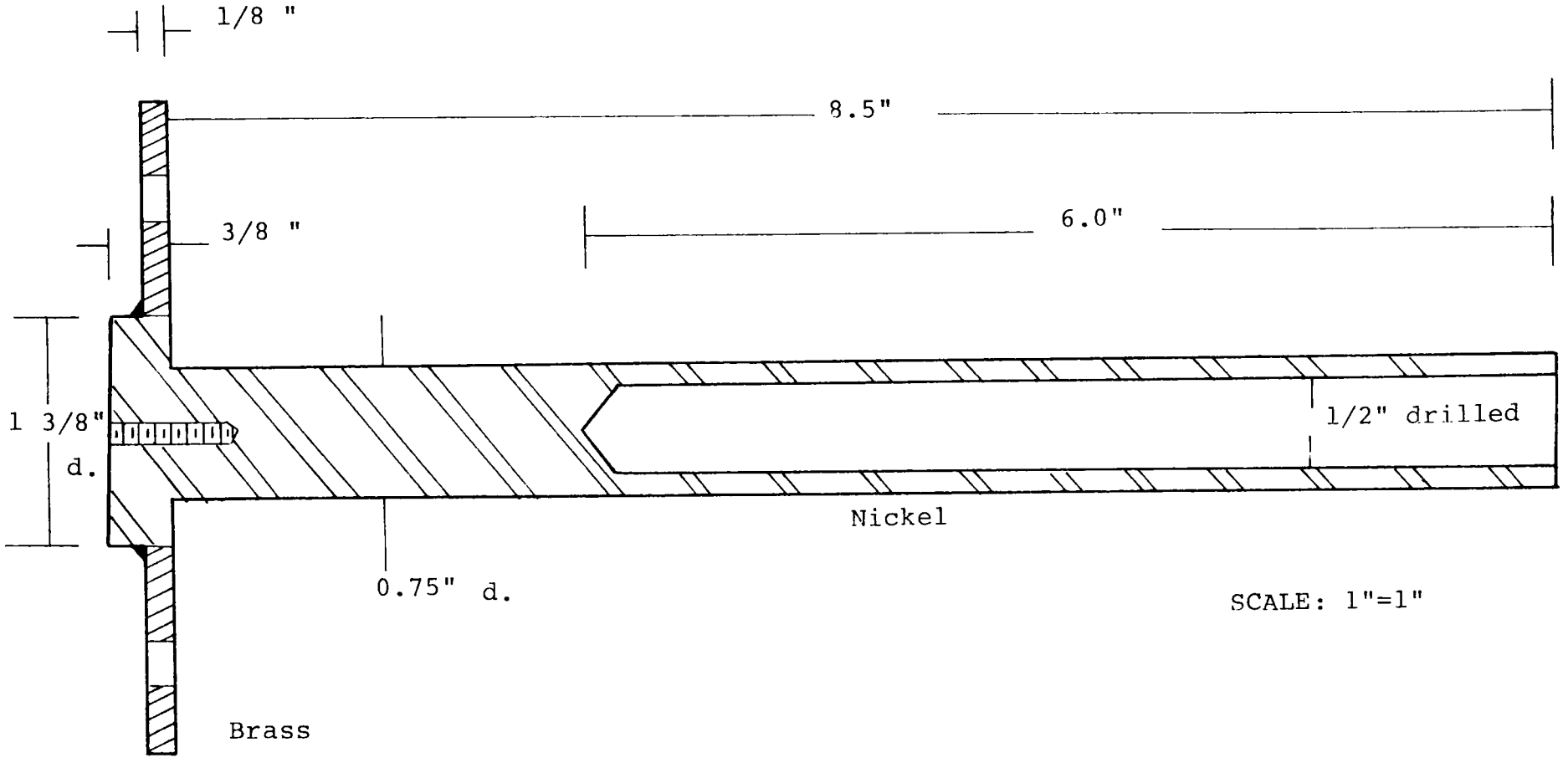

Figure 11.

The argon ion laser cold cathode.

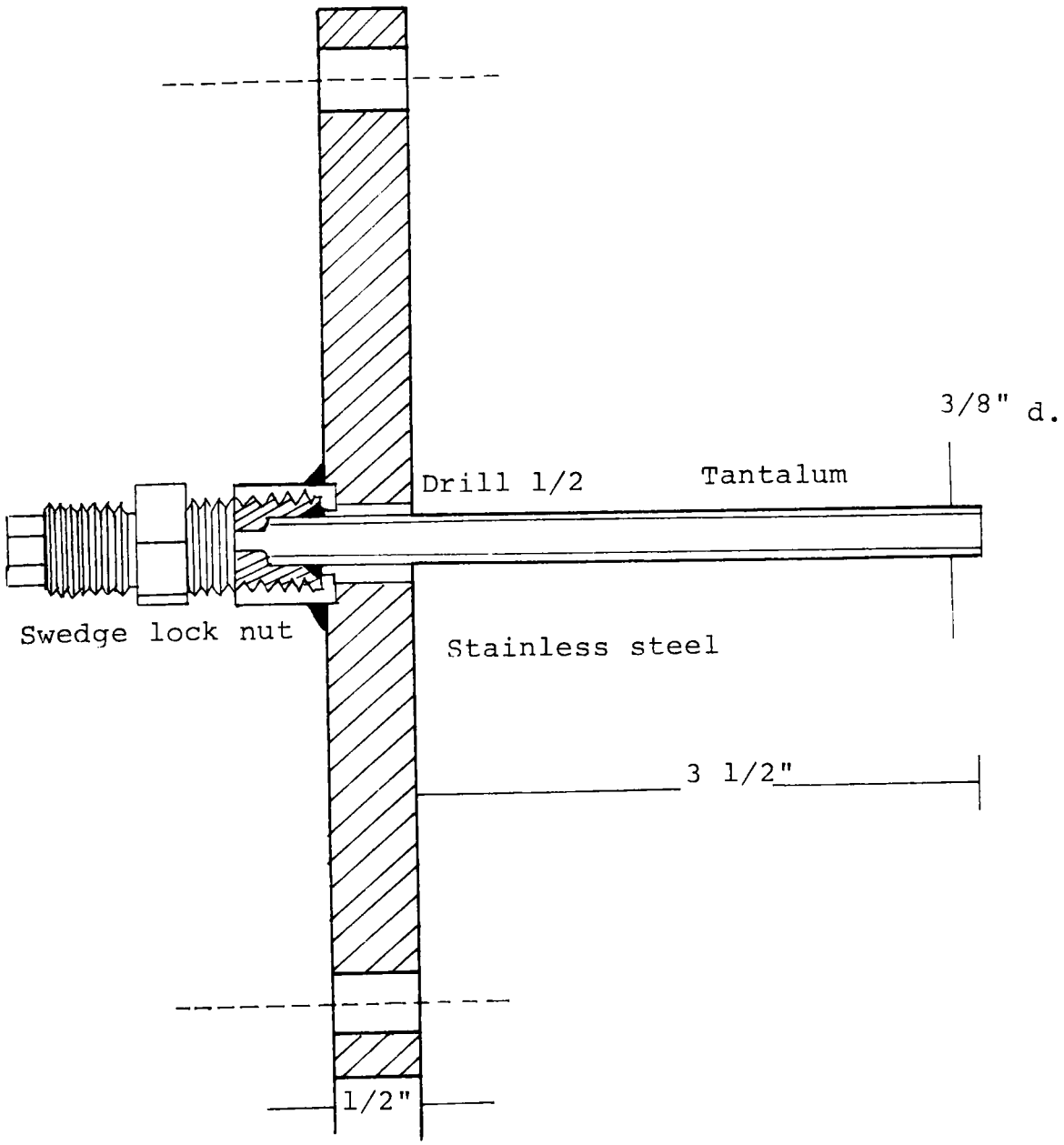

Figure 12.

The side view of the argon ion laser anode.

The mirrors of 2 meters focal length were of high reflectivity broad band in the 3000-5500 Å spectral region. The output mirror,obtained by Oriel Optics had 2 percent transmission. The mirrors are mounted on the standard laser mounts with a high degree of azimuthal and jaw control. The axial alignement of the laser mirrors was obtained by using a helium-neon laser.

The cold cathode, consisting of a hollow nickel cylinder immersed in magnetic field, was used(Figure 11). The anode was a hollow tantalum cylinder, which has been, as well as the cold cathode, put together with the "o" rings(Figure 12). The argon ion laser was immerged into a magnetic field, consisting of the series of Helmholtz coils. Typical values for coil currents were about 22 A, producing a central field in excess of 400 Gauss. The magnetic field was directed from the cathode towards the anode, and it was not fully regulated.

5. Vacuum system

The entire envelope of the vacuum system was made from 3" and 1" pyrex conical pipe connected with the viton "o" rings. This envelope was connected to the diffusion pump

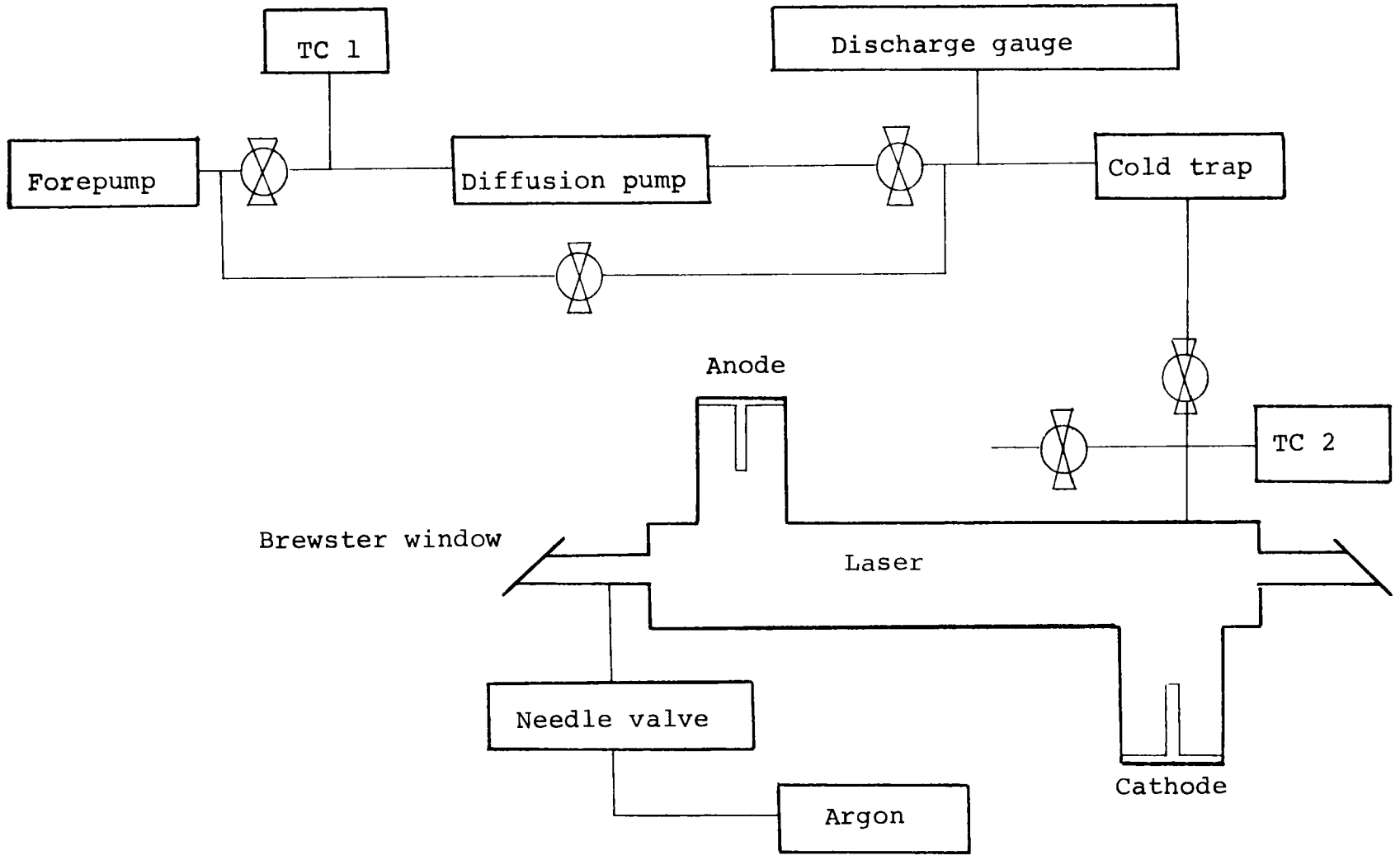

Figure 13.

Block diagram of the vacuum system.

via bellows(Figure 13). Basically, the vacuum system was a forepump with a bypass valve to a CVC diffusion pump. The base pressure was measured and found to be about 5.0×10^{-6} Torr.

The gas used in the study was Ar (99.999% pure), obtained by Matheson Co. Inc. Maximum impurity was about 10 parts per million, mostly due to the presence of other inert gases such as helium and neon.

CHAPTER V

RESULTS AND CONCLUSION

1. Efficiency of the detection system

The spectral radiance P_{16} as a function of the wavelength and the temperature was known from Jobe's data[24]. By measuring the detector current I_{SL} in 3500-5500 Å spectral region for a known temperature of the standard lamp, the efficiency of the detection system to a multiplicative constant D was found using equation (4-16). Since the efficiency should not depend on the intensity of the observed radiation, the detector current measurement was run for a series of temperatures: 1600, 1800 and 2000 $^{\circ}$K, respectively. When only the notch of the standard lamp was observed, the three curves were identical(Figure 14). When the notch was viewed with the rest of the filament the curves were different which was attributed to the large temperature gradient of the rest of the filament.

2. Folded cross sections and their ratios

Folded cross sections for eight argon ion laser transitions were found by using the computer program

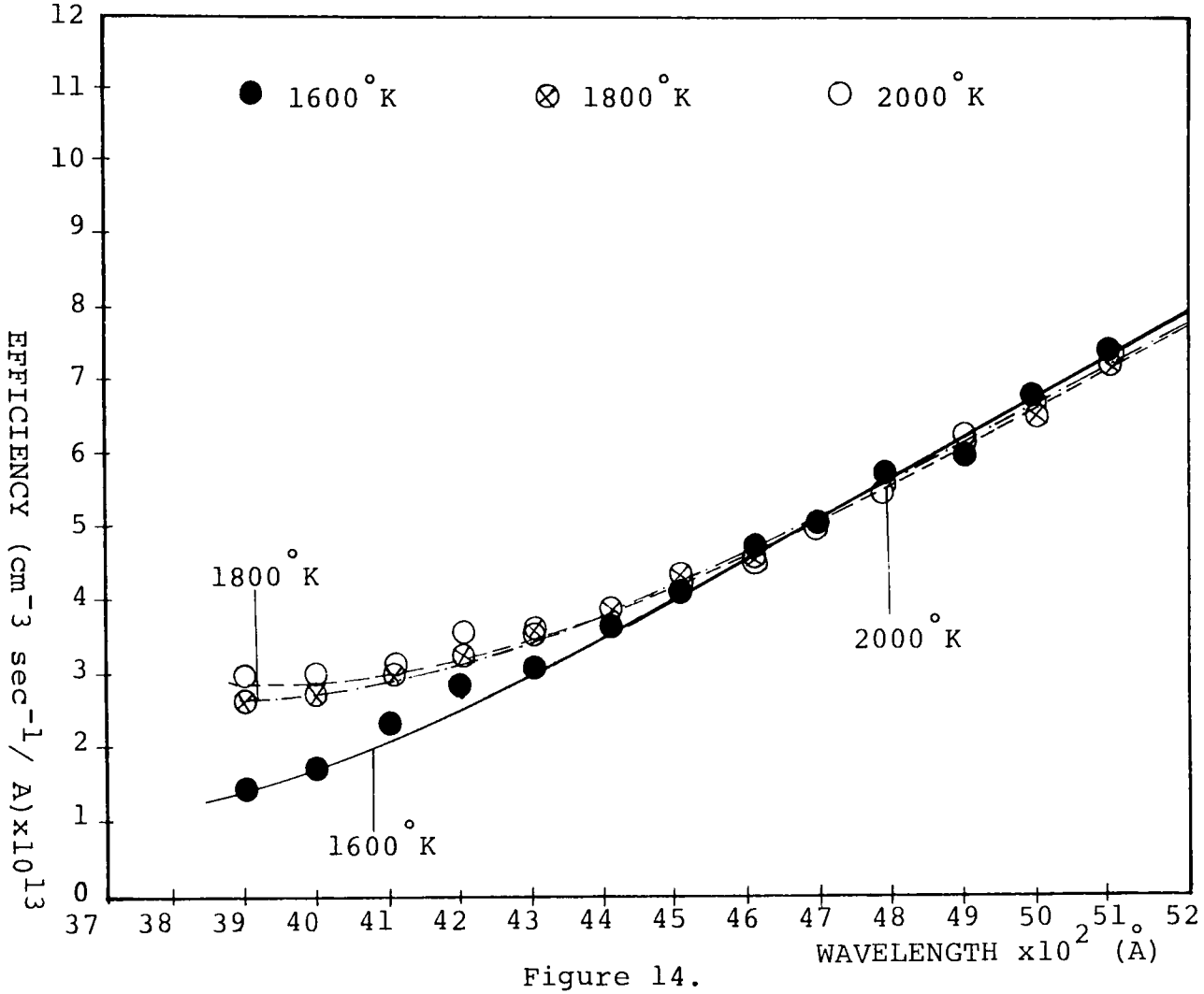

Figure 14.

The efficiency of experimental detection system as a function of wavelength for three different temperatures.

(see Appendix). Then the ratio R was found for each of the folded cross sections with the remaining seven using equation (2-31), and was plotted as a function of the electron temperature T_e. The curves were theoretical line intensity ratios from which the electron temperature was later deduced by the spectroscopic measurement of the line intensity ratio R'. We considered only these curves $R=f(T_e)$ for which a significant change in the value of R does not considerably affect the electron temperature T_e. We noted, that some of the line intensity ratio curves were esssentially insensitive functions of the electron temperature, which was attributed to the similarity in the cross sections appearing in the ratio R. Four of the more sensitive curves representing the ratio of the folded cross sections used to obtain the electron temperature are shown in Figure 15a and Figure 15b. The 4p-4s transitions making the ratio R in Figure 15a have different cross section curves.

3. Experimentally observed line intensities

The line ratio technique, adopted for the measurement of the electron temperature, depends upon the intensity of the sidelight in the spectral line.(the sidelight is the light radiated in the direction transverse to the

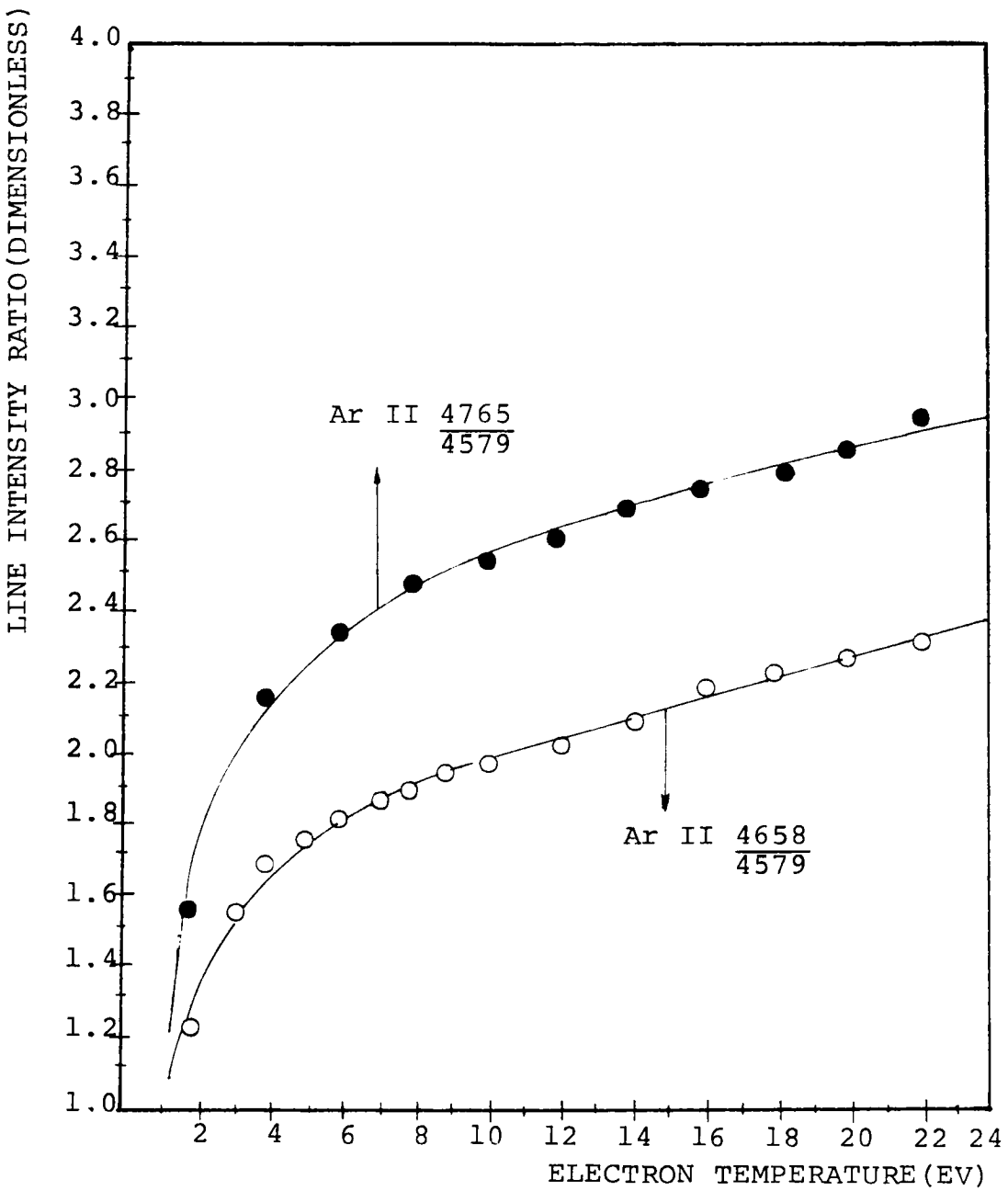

Figure 15a.

The ratio of folded cross sections as a function of electron temperature for some Ar II lines.

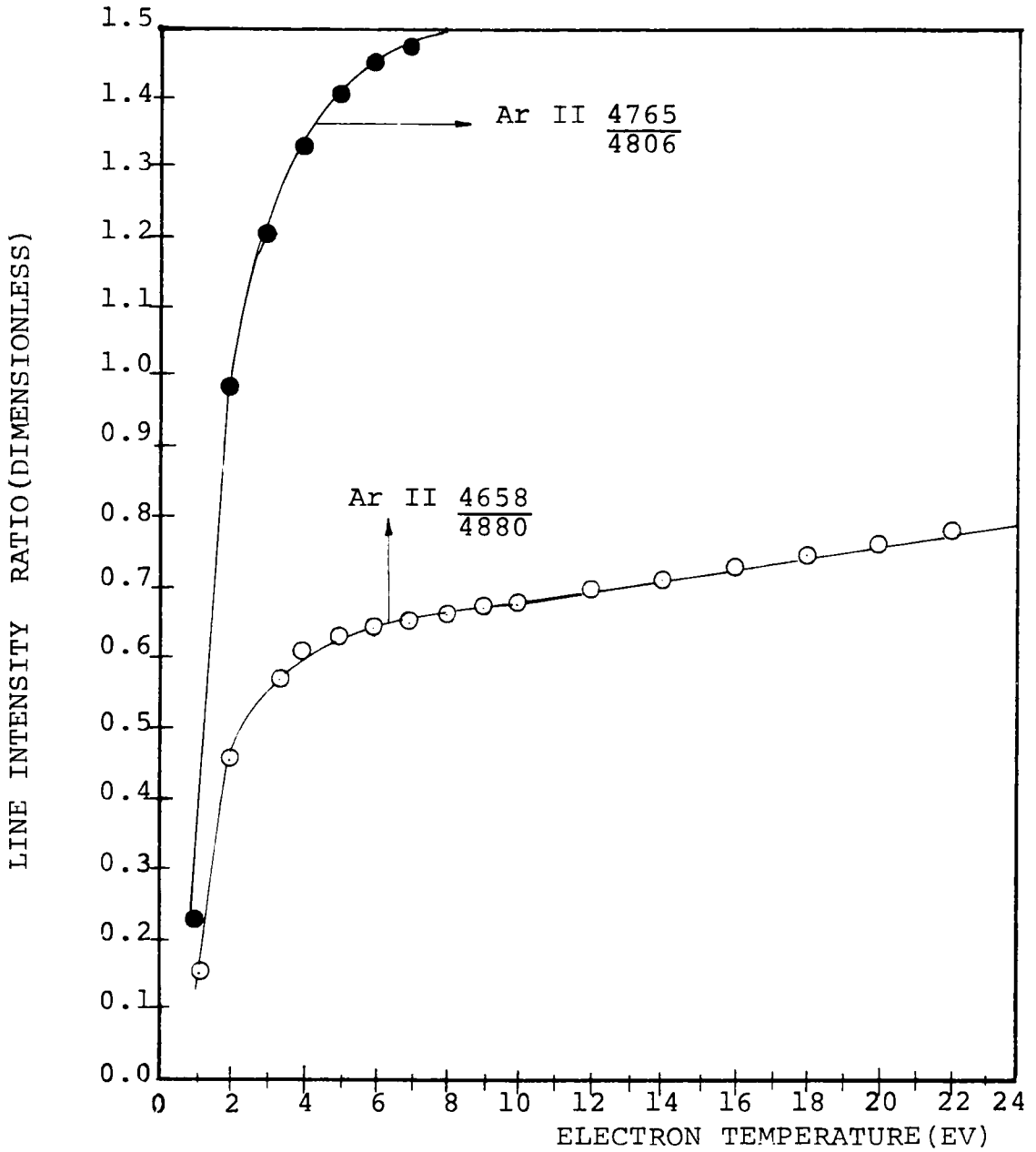

Figure 15b.

The ratio of folded cross sections as a function of electron temperature for some Ar II lines.

laser axis.) The rate equations described in Chapter II remain valid, as long as the simultaneous excitation and ionization, together with the cascading processes, is considered as the dominant populating mechanism of the upper laser states. The time interval during which they remain valid depends on the parameters such as: pressure, current, temperature and the repetition rate.(since the metastable levels can also be involved.) The sidelight intensity measurements were performed by using the identical optics as used in the calibration procedure. The same slit widths and solid angles were used, such that the relative line intensities could be measured. The peak sidelight intensities of all the lines were measured at the same time, namely 30 μsec from the beginning of the capacitive discharge. The absolute intensities were found from the relative intensities using the previously obtained efficiency curve. The observed sidelight intensities of the 4806 Å line and the 4579 Å line are shown in Figure 16a and Figure 16b. Figure 17 shows the current through the laser and the output power of the 4880 Å line as functions of time. The sidelight follows the current in the tube, but the lasing pulse is delayed from the onset value of the current by 30-35 μsec. The time dependence of the current through the tube and the voltage drop across the tube are shown

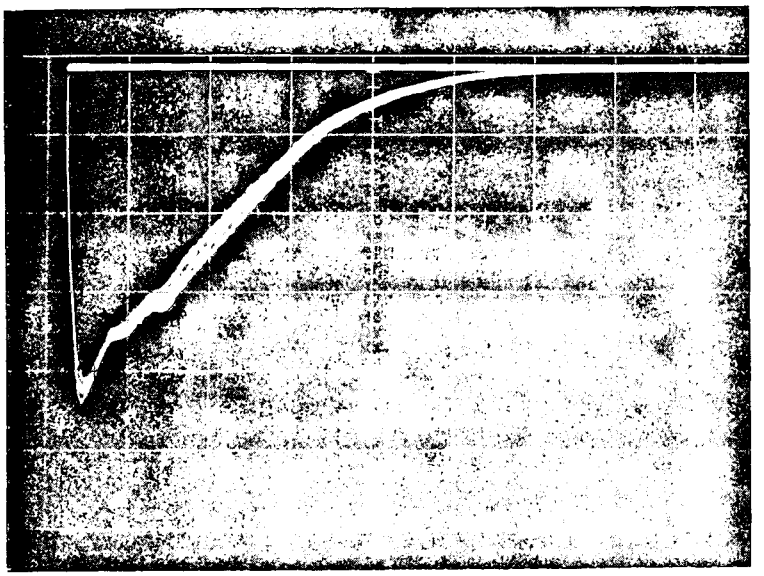

Figure 16 a.

The sidelight intensity of the 4806 Å line as the function of the time. Vertical deflection: 10 V/cm;time base: 100μsec/cm.

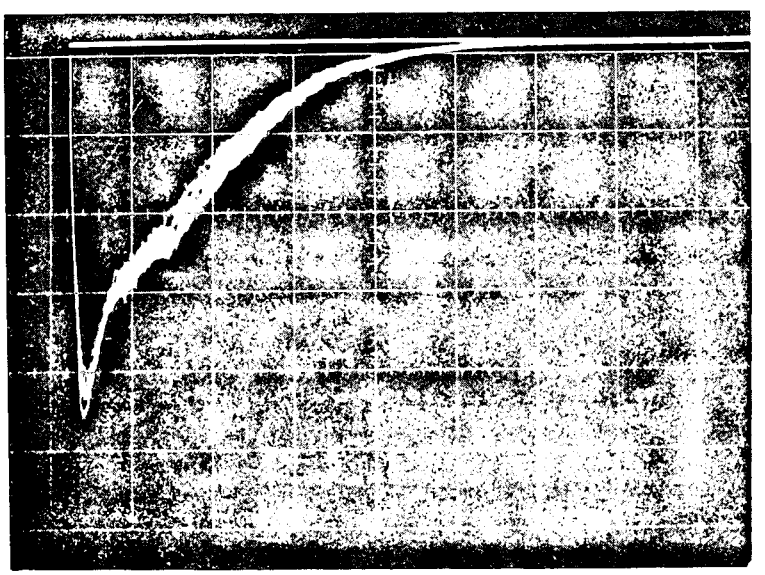

Figure 16 b.

The sidelight intensity of the 4579 Å line as the function of the time. Vertical deflection: 2 V/cm;time base: 100μsec/cm.

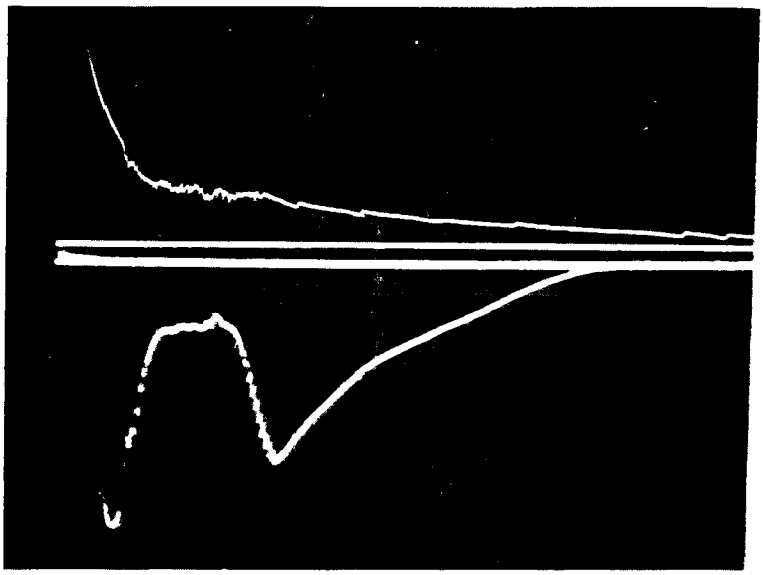

Figure 17.

The current and the output power of the 4880 Å line as the function of the time. Top: current 20 A/cm; bottom: EGG detector,no neutral density filter. Same time base: 50 μsec/cm.

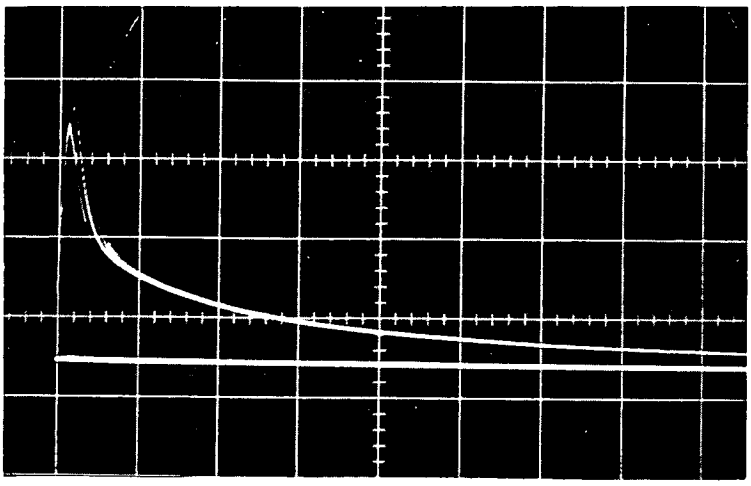

Figure 18.

The time dependence of the current through the tube. Current pulse 20 A/cm,time base 10 μsec/cm,115 μHg argon pressure.

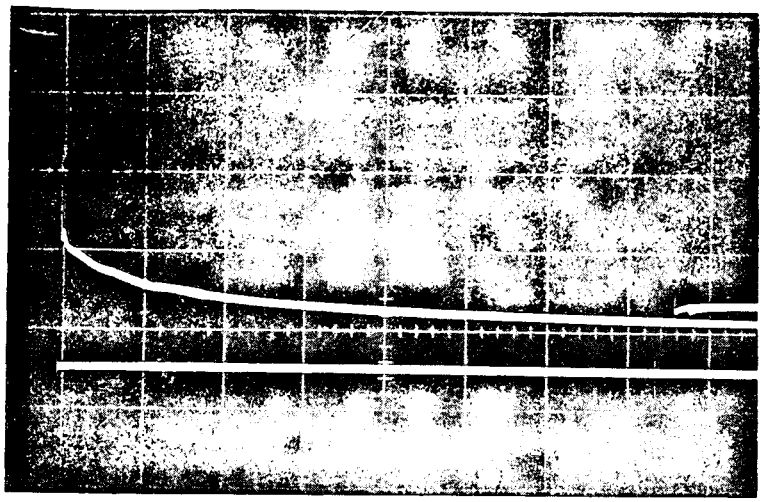

Figure 19.

The voltage drop across the tube during the pulse. Vertical deflection: 500 V/cm; time base: 100 μsec/cm, 110 μ pressure.

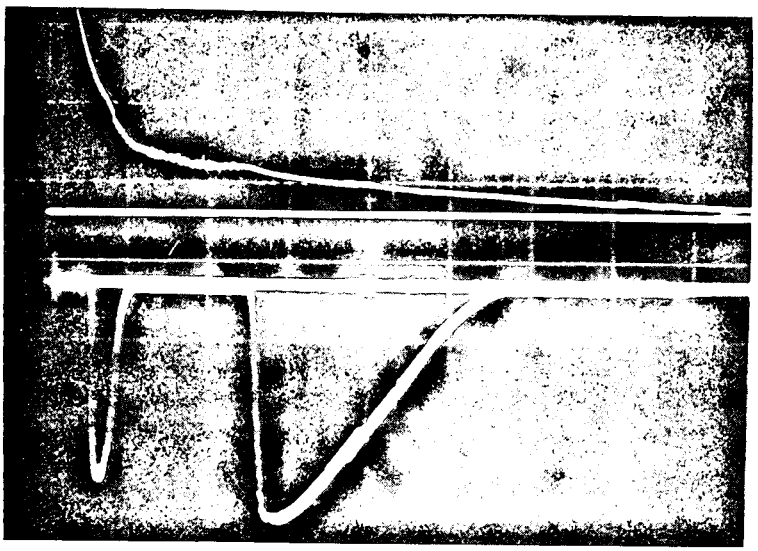

Figure 20.

The time dependence of the laser pulse for the 4765 Å line. Top: current 20 A/cm; bottom: EGG detector 5 mV/cm, time base: 50 μsec/cm, repetition rate 3 p.p.s.

in Figure 18 and Figure 19. The time dependence of the output laser pulse for the 4765 Å line is shown in Figure 20. The appearance of the two pulses for this line is observed. The 4880 Å and 5145 Å spectral lines also exhibit two spikes, whereas the 4965 Å has only one. The lasing action does not begin until the current falls to the level of approximately 40-50 A, and then continues until the current dies out significantly. The measured(to a multiplicative constant D) absolute intensities of the spectroscopically observed Ar I and Ar II lines in the pulsed argon ion laser discharge are shown in Table I. Only the eight lines for which the cross sections are available can be used to determine the electron temperature. The ratios of the line intensities for the transitions studies by Latimer and St. John are displayed in Table II. By using the suitable theoretical ratios of the folded cross sections one can now determine the electron temperature. From most of the curves, we obtained the electron temperature values ranging from 1.0-1.75 eV.

4.Electron temperature

A comparison can be made with a Tonks-Langmuir relation

Wavelength (Å) ①	Deflection (cm) ②	Scale used (V/cm) ③	Actual (V/cm) ④	Intensity (V) ⑤ ② × ④	Efficiency at 2000°C ($cm^3 sec^{-1} A^{-1}$) ⑥	Absolute intensity ($cm^{-3} sec^{-1}$) ⑦ ⑤ × ⑥
3850.58	4.14	5	5.13	21.24	3.0	63.72
4348.06	3.12	20	20.62	64.30	3.8	244.34
4426.01	4.21	10	10.47	44.08	4.1	180.73
4579.35	4.83	2	2.04	9.84	4.7	45.75
ArI 4596.10	3.71	0.2	0.20	0.75	4.8	3.56
4609.56	4.59	5	5.13	23.55	4.8	113.00
4657.89	2.02	5	5.13	10.36	5.0	51.80
4726.86	2.57	5	5.13	13.18	5.3	69.85
4735.91	2.81	10	10.47	29.42	5.3	156.20
4764.86	2.44	5	5.13	12.49	5.5	68.07
4806.02	4.36	10	10.47	45.65	5.7	259.29
4879.86	2.84	10	10.47	29.68	6.0	177.19
4965.07	3.86	2	2.04	7.87	6.5	50.76
5009.33	2.31	5	5.13	11.85	6.7	79.15
5017.16	4.50	1	1.04	4.67	6.8	31.52
5062.04	2.20	5	5.13	11.26	7.1	79.72
5145.32	2.76	2	2.04	5.63	7.7	43.07

Table I.

The absolute intensities of the Ar I and Ar II lines observed in the laser discharge.

Remark: the ratio in the Table II = $\frac{\text{intensity of the line in vertical column}}{\text{intensity of the line in horizontal row}}$

$ArII_{o}$ LineA	3850	4426	4579	4658	4765	4806	4880	4965
3850	xxxx	2.84	0.72	0.81	1.07	4.07	2.78	0.80
4426	0.35	xxxx	0.25	0.29	0.38	1.43	0.98	0.28
4579	1.39	3.95	xxxx	1.13	1.48	5.66	3.87	1.11
4658	1.23	3.49	0.88	xxxx	1.31	5.00	3.42	0.98
4765	0.94	2.65	0.67	0.76	xxxx	3.81	2.60	0.75
4806	0.25	0.70	0.18	0.20	0.26	xxxx	0.68	0.20
4880	0.36	1.01	0.26	0.29	0.38	1.46	xxxx	0.29
4965	1.25	3.56	0.90	1.02	1.34	5.11	3.49	xxxx

Table II.

Experimentally obtained intensity ratios of argon ion lines.

for the low pressure, weakly ionized positive column. If the single step ionization is assumed, one has (26)

$$\left(1 + \frac{k\,T_e}{e\,V_i}\right)^{-1} \exp\left(\frac{e\,V_i}{k\,T_e}\right) = 62.8\; a\; V_i \sqrt{M}\; pR \qquad (5\text{-}1)$$

In equation (5-1), V_i is the ionization potential; a is the differential ionization coefficient of the gas at the pressure of 1 Torr; M is the molecular weight; R is the radius of the discharge tube; and k is the Boltzmann constant. The electron temperature T_e in equation (5-1) does not depend on the discharge current, and it is only the function of the bore radius and the gas pressure. With the known constants for the argon gas (a=o.71, V_i=15.755 eV, M=39.9) and the experimental parameters p=0.11 Torr and R=0.356 cm for this laser, one can estimate from the transcendental equation (5-1), 3.1 eV value for the electron temperature.

Another comparison can be made with the theory of the positive column by v. Engel and Steenbeck (6) (Figure 20a). The value of the constant C for the argon gas is 5.3×10^{-2}, V_i=15.755 eV and pR factor is 3.85×10^{-2} Torr cm. From the Figure 20a one can obtain 3.0 eV for the electron temperature value.

The electron temperature in the high current density (2000 A/cm^2) in the pulsed argon ion laser was measured with a double probe method by Hattori and Goto[11]. The pressure values were ranging from 15 to 50 mTorr, much smaller then in this experiment; and the bore diameter was 6 and 10 mm. Their results are shown in Figure 20b. It is expected from the shape of the family of curves in this diagram, that at a lower current density and larger pressure values, the electron temperature may be close to 2 eV.

Finally a comparison can be made with the data(shown below) of Zarowin, who calculated the electron temperature in the continuous argon ion laser discharge[29]. Zarowin's results indicate that the electron temeprature is proportional to the 2/3 power of the current density.

Current density(A/cm^2)	Electron temperature (eV)
25	1.0
120	3.0
250	4.7
500	7.5

In this experiment the current was about 20-30 A(the peak current was 250 A),and the electron temperature using

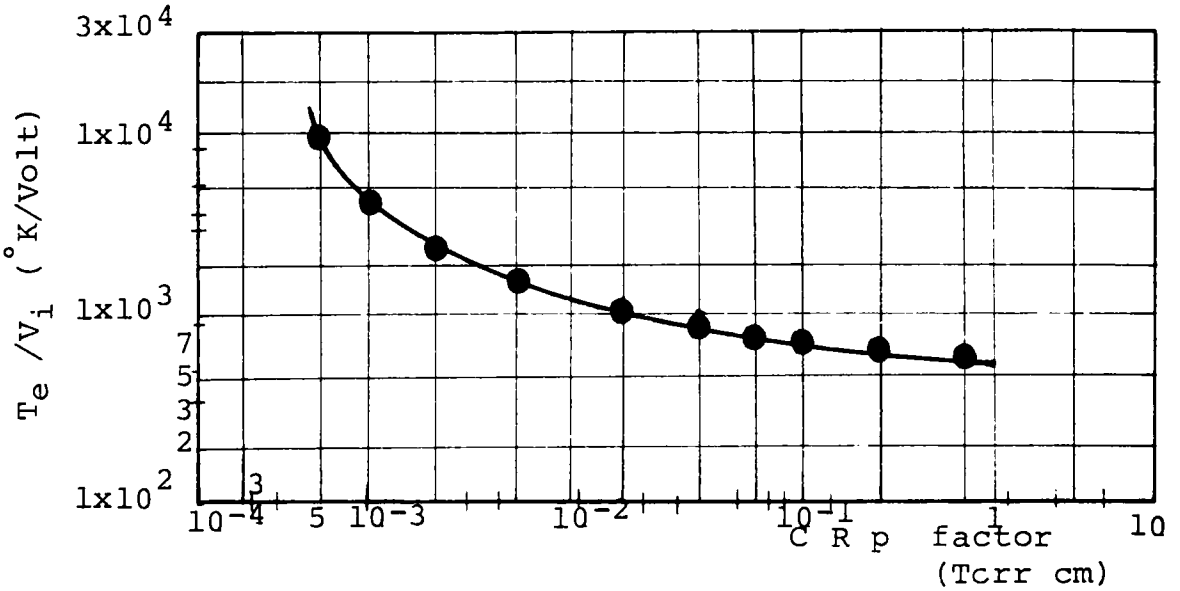

Figure 20a.

The electron temperature as a function of Rp factor(after v. Engel and Steenback)

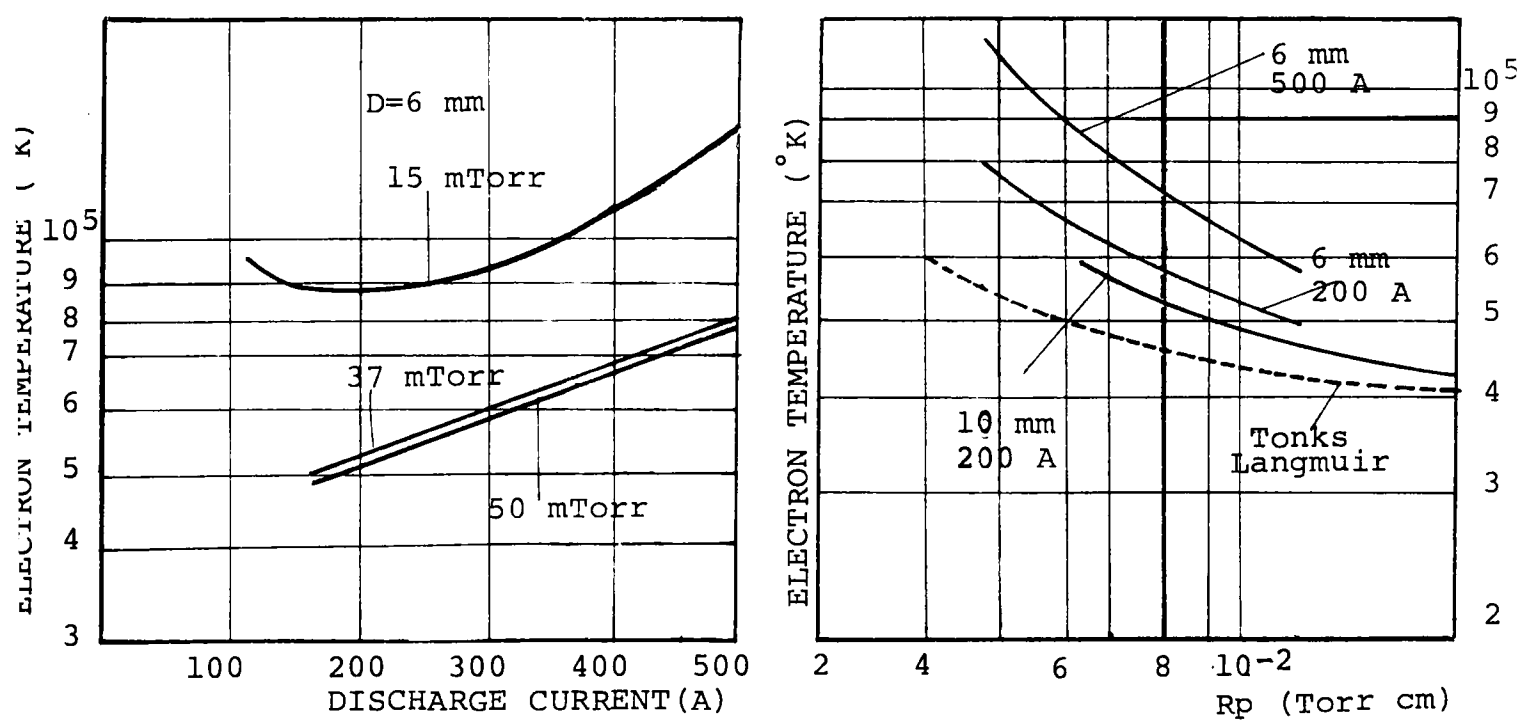

Figure 20b.

The experimental results of Hattori and Goto

Zarowin's data is found to be about 2.0-3.0 eV.

5. Conclusion

The electron temperature value obtained by the line intensity ratio technique is lower then indicated by theoretical predictions [6,26,29], which probably indicates that there is an additional mechanism for the population of the upper laser states in addition to the assumed single step excitation and ionization. Due to its large cross section(10 times larger than the same for the neutral ground state excitation) and low ionization treshold, it is believed that the lowest neutral metastable state $^3P^0$ 4s'[1/2]$_0$ at the energy level of 11.548 eV from the neutral ground state, might be the favorable level for the ionization to take place. It is more likely that the quartets, rather than the doublets in the upper laser states will be populated by the excitation from the metastable neutral level. In Figure 15a, the ratio of a doublet 4765 Å to a quartet 4806 Å line was plotted as a function of the electron temperature. If the excitation from the metastable level is also considered as a populating mechanism for the quartet levels, an additional term accounting for this process (and therefore contribution to the intensity) has to be added to folded cross section for single step excitation and ionization. The ratio curve of $\frac{4765}{4806}$ folded cross sections will be lo-

wered, and one would measure the larger values for the electron temperature using the same observed absolute line intensity ratios from Table II. The experiment is suggested in which the metastable level would be quenched(adding krypton to the argon gas), and therefore the excitation from this level as a possible populating mechanism for the quartet upper laser levels would be negligible.

*

The line intensity technique for the measurement of the electron temperature was applied to the tenuous plasma in the argon ion laser. Estimates of the electron temperatures were made, based on the assumption that the upper laser levels are populated by a single step excitation and ionization process. The resulting temperatures were one and a half to two times lower than measured by another diagnostic method and other theoretical predictions, suggesting that the single step excitation and ionization is not the dominant process in the pulsed device used.

APPENDIX

The FORTRAN II program was written to compute the folded cross sections. Latimer's and St. John's value pairs for the electron energy and the corresponding cross section were punched on the data cards. The program is folding the known optical effective cross sections over the Maxwellian velocity distribution of the electrons, according to the equation (2-24)

$$\langle Q_{ji}(v)\ v\rangle = \int_{v_j}^{\infty} Q_{ji}(v)\ f(v)\ v\ dv, \quad (2\text{-}24)$$

and the electron temperature is ranging from 1-25 eV. The simple trapezodial integration subroutine was used. The folded cross sections and the corresponding electron temperature were printed as an output. The flow chart and the sample source program are shown in Figure 21 and Figure 22. The computer program was checked by calculating the mean velocity $\bar{v}$. It is easily seen, that the relation for the mean velocity is obtained from the expression for the folded cross section(2-24), if the latter is set to be equal to one, namely[20]

$$\bar{v} = \frac{\int_0^{\infty} v\ f(v)\ dv}{\int_0^{\infty} f(v)\ dv} \quad (1)$$

The mean velocity $\bar{v}$ is a function of the temperature only, as[20]

$$\bar{v} = \left(\frac{8kT}{m}\right)^{1/2} \quad . \qquad (2)$$

Additional checking was done, by testing the computer program for the calculation of the root mean square velocity v_R, as [20]

$$v_R = \frac{\int_0^\infty v^2 f(v)\, dv}{\int_0^\infty f(v)\, dv} = \left(\frac{3kT}{m}\right)^{1/2} \quad . \qquad (3)$$

The relation(3) is obtained from equation(2-24) by setting the velocity numerically equal to the cross section. The values for $\bar{v}$ and v_R obtained by the computer program were compared with the values calculated from equations (2) and (3), and excellent agreement was observed.

1. FLOW CHART DIAGRAM OF THE COMPUTER PROGRAM FOR CALCULATION OF FOLDED CROSS SECTIONS

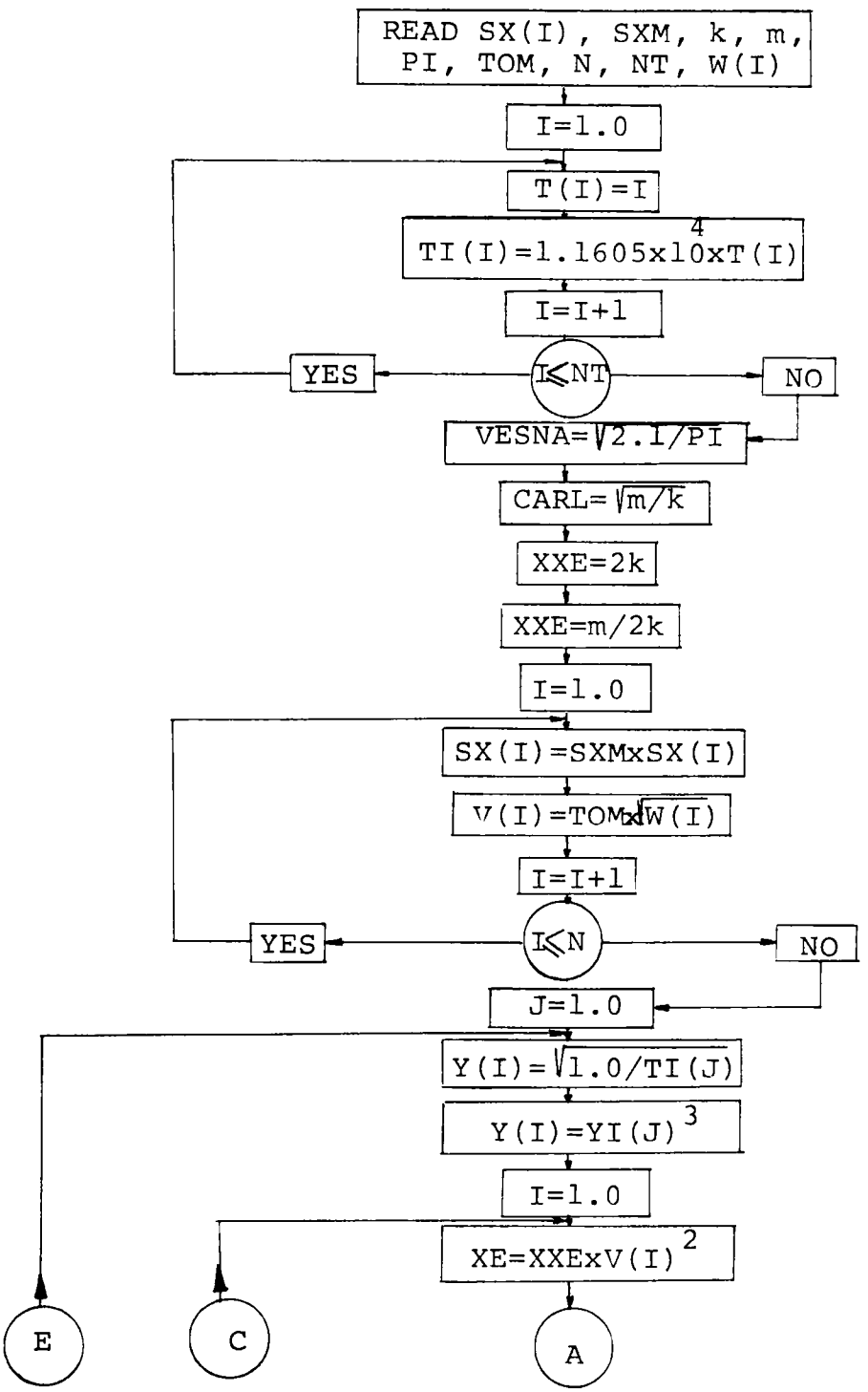

Figure 21.

Flow chart diagram of the computer program for calculation of folded cross sections.

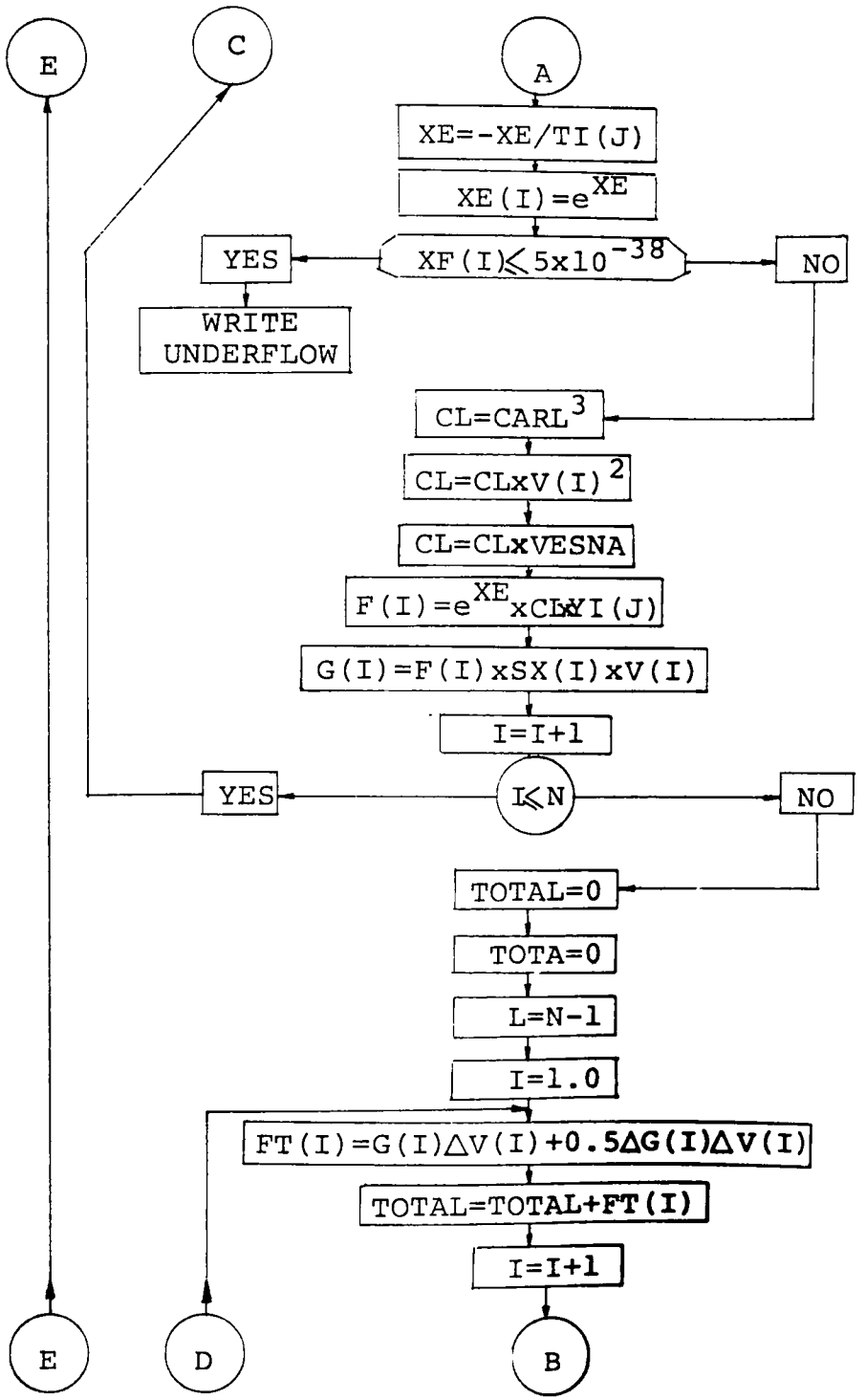

Figure 21.

(continued)

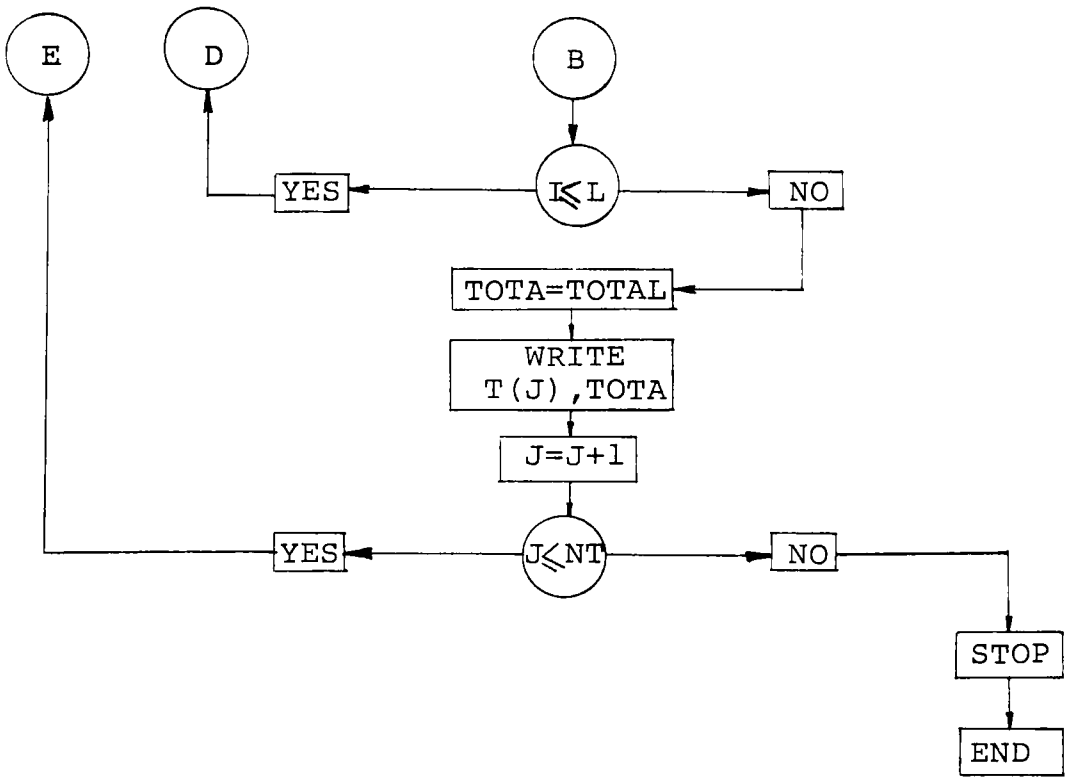

Remark: the symbol k in the flow chart is called BOLCO in the FORTRAN II program
the symbol m in the flow chart is called ELMAS in the FORTRAN II program
SX(I) is cross section in cm^2
W(I) is the electron energy in eV
k is Boltzmann constant 1.38×10^{-16} erg K^{-1}
m is the electron mass 9.11×10^{-28} g
T(I) is the electron temperature in eV
TOM is the velocity corresponding to 1 eV electron energy
N is maximum number of cross sections
NT is maximum number of temperature of electrons

Figure 21.

(continued)

```
*ONE WORD INTEGERS
*LIST SOURCE PROGRAM
*EXTENDED PRECISION
*IOCS(CARD,1132 PRINTER)
      DIMENSION V(40),W(40),SX(40),XF(40),F(40),FT(40),G(40),T(25),
     1YI(25),TI(25)
      N=40.0
      BOLCO=1.38049*1.0E-16
      ELMAS=9.1086*1.oE-28
      PI=3.1415927
      TOM=0.593090*1.0E8
      NT=25.0
      WRITE (3,77)
 77   FORMAT(20X,'AVERAGE OF CROSS SECTION OVER MAXWELLIAN')
      WRITE (3,78)
 78   FORMAT(30X,'ARGON ION RESULTS')
      WRITE (3,79)
 79   FORMAT(17X,'TEMPERATURE',5X,'FOLDED CROSS SECTIONS')
      WRITE (3,80)
 80   FORMAT(22X,'EV',14X,'CM**3 SEC-1')
      TOTAL 0.0
      DO 13 I=1,NT
 13   T(I)=I
      DO 14 I=1,NT
 14   TI(I)=1.1605*1.0E4 * T(I)
      READ (2,1000) (W(I),SX(I),I=1,N)
1000  FORMAT (8F10.0)
      WRITE (3,908) (W(I),SX(I),I=1,N)
 908  FORMAT(1H,8F10.5)
      VESNA=SQRT(2.0/PI)
      CARL=SQRT(ELMAS/BOLCO)
      XXE=2.0*BOLCO
      XXE=ELMAS/XXE
      DO 11 I=1,N
C     CROSS SECTIONS ARE FOR 4765 ÅNGSTROMS LINE
      SX(I)=SX(I)*52.0*1.0E16
C     52.0 IS THE CROSS SECTION PEAK;1.0E16 ARBITRARY CONSTANT
 11   V(I)=TOM*SQRT(W(I))
      DO 15 J=1,NT
      YI(J)=SQRT(1.0/TI(J))
      YI(J)=YI(J)*YI(J)*YI(J)
      DO 16 I=1,N
      XE=XXE*V(I)*V(I)
      XE=-XE/TI(J)
      XF(I)=EEXP(XE)
      IF (XF(I)-5.0*1.0E-38)  45,45,111
 45   WRITE (3,72)
 72   FORMAT(5X,'UNDERFLOW',10X,'I',10X,'J')
      WRITE (3,73) I,J
 73   FORMAT(20X,I5,6X,I5)
```

Figure 22.

FORTRAN II program for calculation of folded cross sections.

```
 111  CL=CARL*CARL*CARL
      CL=CL*V(I)*V(I)
      CL=CL*VESNA
      F(I)=XF(I)*CL*YI(J)
      G(I)=F(I)*V(I)*SX(I)
  16  CONTINUE
C     TRAPEZODIAL INTEGRATION ROUTINE
      TOTAL=0.000
      TOTA=0.000
      L=N-1
      DO 17 I=1,L
      FT(I)=G(I)*(V(I+1)-V(I)+0.5(G(I+1)-G(I))*(V(I+1)-V(I))
  17  TOTAL=TOTAL+FT(I)
      TOTA=TOTAL
      WRITE(3,81) T(J),TOTA
  81  FORMAT(21X,F5.2,15X,E12.4)
  15  CONTINUE
      CALL EXIT
      END


 FEATURES SUPPORTED
 ONE WORD INTEGERS
 EXTENDED PRECISION
 IOCS

 CORE REQUIREMENTS FOR
  COMMON       0  VARIABLES     1112  PROGRAM  706
 END OF COMPILATION
 // XEQ

 ENTER NUMBER OF CROSS SECTIONS
                    AVERAGE OF CROSS SECTIONS OVER MAXWELLIAN
                              ARGON ION RESULTS
                  TEMPERATURE FOLDED CROSS SECTIONS
                       EV            CM**3 SEC-1

  35.4400 0.0000  40.0000 0.4080  45.0000 0.6520  50.0000 0.8720
  55.0000 0.9040  60.0000 0.9180  65.0000 0.9280  70.0000 0.9440
  75.0000 0.9540  80.0000 0.9630  85.0000 0.9180  86.0000 0.9840
  87.0000 0.9860  88.0000 0.9890  90.0000 1.0000  91.0000 0.9950
  92.0000 0.9880  93.0000 0.9830  94.0000 0.9780  95.0000 0.9760
 100.0000 0.9440 105.0000 0.9120 110.0000 0.8960 115.0000 0.8760
 120.0000 0.8600 125.0000 0.8400 130.0000 0.8210 135.0000 0.8060
 140.0000 0.7850 145.0000 0.7720 150.0000 0.7530 155.0000 0.7360
 160.0000 0.7210 165.0000 0.7060 170.0000 0.6910 175.0000 0.6720
 180.0000 0.6560 185.0000 0.6410 190.0000 0.6270 194.0000 0.6200
```

Figure 22.

(continued)

```
UNDERFLOW          I           J
                  12           1
UNDERFLOW          I           J
                  13           1
.........        ....        ....
UNDERFLOW          I           J
                  40           1

                 1.00                    0.1168E 11
UNDERFLOW          I           J
                  36           2
.........        ....        ....
UNDERFLOW          I           J
                  40           2
```

```
 2.00          0.2324E 19
 3.00          0.1254E 22
 4.00          0.2894E 23
 5.00          0.1904E 24
 6.00          0.6695E 24
 7.00          0.1644E 25
 8.00          0.3227E 25
 9.00          0.5455E 25
10.00          0.8301E 25
11.00          0.1170E 26
12.00          0.1559E 26
13.00          0.1986E 26
14.00          0.2445E 26
15.00          0.2927E 26
16.00          0.3426E 26
17.00          0.3935E 26
18.00          0.4451E 26
19.00          0.4968E 26
20.00          0.5483E 26
21.00          0.5993E 26
22.00          0.6496E 26
23.00          0.6989E 26
24.00          0.7472E 26
25.00          0.7942E 26
```

Figure 22.

(continued)

REFERENCES

1. J. K. Ballou, C. C. Lin, private communication.
2. K. M. Bell, E. J. Powers, Technical Memorandum, 2, (Sept. 1968), The University of Texas at Austin.
3. W. R. Bennett, Jr., G. N. Mercer, P. J. Kindlmann, B. W. Wexler, and H. Hyman, Phys. Rev. Letters 17, 987 (1966).
4. W. R. Bennett, Jr., J. Appl. Phys. Letters, 10, 177 (1967)
5. P. N. Clout, D. W. O. Heddle, Sixth Int. Conf. on Phys. of Elec. and Atomic Collissions,(Cambridge, Massachussets 1969, p.290)
6. J. D. Cobine, Gaseous Conductors Theory and Engineering Applications, Dover Publications, Inc. New York 1958, p.240.
7. S. P. Cunningham, U. S. Atomic Energy Commission, Rep. WASH - 289, p. 279 (1955).
8. J. C. DeVos, Physica 20, 690 (1945).
9. S. E. Frish, NASA TT F-457, p.1 (1967).
10. J. M. Hammer, C. P. Wen, J. Chem. Phys. 46, 1225 (1967)
11. S. Hattori, T. Goto, IEEE J. Quant. Elec. QE-5, 531 (1969)
12. J. D. Jobe, Ph. D. Dissertation, University of Oklahoma, Norman, Oklahoma (1968)

13. H. J. Kostowski, R. D. Lee, Precision Measurement and Calibration Temperature, Ed. J. F. Swindells, NBS Special Publication 300, 2, 363 (1968).

14. S. H. Koozekanani, IEEE J. Quant. Elec. QE-2, 770 (1966)

15. S. H. Koozekanani, Appl. Phys. Letters, 11,No.3, 106 (1967)

16. E. F. Labuda, E. I. Gordon, R. C. Miller, IEEE J. Quant. Elec. QE-1, 273 (1965)

17. E. F. Labuda, C. E. Webb, R. C. Miller,E. I. Gordon, "A Study of Capillary Discharge in Noble Gases at high Current Densities",presented at the 18th Gaseous Electronic Conference, Minneapolis, Minnesota, 1965.

18. I. D. Latimer, R. N. St. John, Phys. Rev. Ser.A.1, 1612 (1970)

19. J. H. Lees, Proc. Roy. Soc. (London) A137, 173 (1943)

20. E. W. McDaniel, Collision Phenomena in Ionized Gases, J. Wiley & Sons, Inc. New York, 1964, p.34.

21. R. I. Rudko, C. L. Tang, Appl. Phys. Letters, 9, 41 (1966)

22. F. W. Sears, An Introduction to Thermodynamics, the Kinetic Theory of Gases and Statistical Mechanics, (Addison-Wesley, Reding, Massachussets, 1964, p.239)

23. R. J. Sovie, Physics of Fluids (USA), 7, 613 (1964)

24. R. M. St. John, private communication.

25. P. C. Thonemann, Optical Spetroscopic Measurements of High Temperatures, ed. P. J. Dickerman, The University of Chicago Press.

26. L. Tonks, I. Langmuir, Phys. Rev. 34, 876 (1929)

27. R. H. Tourin, Spetroscopic Gas Temperature Measurement, Elsevier, Amsterdam, 1966, p.8.

28. W. L. Wiese, M. W. Smith, B. M. Miles, Atomic Transition Probabilities, Volume II, Sodium through Calcium, U. S. Dept. of Commerce, National Bureau of Standards, NSRDS-NBS 22, 1969, p.204.

29. C. B. Zarowin, Appl. Phys. Letters, 15, p.36 (1969)

VITA

The author was born on March 13, 1943 in Zagreb, Yugoslavia. In June 1961, he was graduated from II Gimnazija "Braća Ribar", Zagreb. In December 1965, he received the diplomed engineer of physics degree from Prirodoslovno-Matematički Fakultet Sveučilišta u Zagrebu (University of Natural and Mathematical Sciences Zagreb). During his undergraduate studies, he spent several summers in Arnhem, The Netherlands, doing research for Koninklijke Nederlandsche Heidemaatschappij. After completition of his undergraduate work, he was employed as a research assistant in the Institute for Thermodynamical and Aerodynamical Research IAT, Zagreb. In November 1968, he was accepted and offered a teaching assistantship at Old Dominion University, Norfolk, Virginia, and entered the Graduate School in February 1969. From the Fall 1969 to the present date, he is working in the Modern Optics and Spectroscopy Laboratory at Old Dominion University.